OPEN ACCESS
International Journal of Structural Stability and Dynamics
(2021) 2150095 (37 pages)

DOI: 10.1142/S0219455421500954

Elastic-Plastic Buckling and Postbuckling Finite Element Analysis of Plates Using Higher-Order Theory

Maciej Taczała*,‡, Ryszard Buczkowski*,§ and Michal Kleiber†,¶

*West Pomeranian University of Technology
71-065 Szczecin, Piastow 41, Poland

†Institute of Fundamental Technological Research
Polish Academy of Sciences
Pawinskiego 5B, 02-106 Warsaw, Poland
‡maciej.taczala@zut.edu.pl
§rbuczkowski@ps.pl
¶mkleiber@ippt.pan.pl

Received 10 November 2020
Accepted 20 February 2021
Published 7 April 2021

In this paper, some of the displacement-based plate theories are used to investigate the elastic-plastic analysis of plates in the framework of the finite element method including the buckling and postbuckling effects with the focus on the general third-order plate theory (GTPT). The plate calculation results were compared with the results obtained using 64-nodes solid elements involving Lobatto integration scheme. The problem is solved using the Newton–Raphson method applying modified Crisfield constant arc-length procedure. The results show good agreement of results and the GTPT can be acknowledged to fulfill essential criteria for application to the elastic-plastic analysis of thin and thick plates.

Keywords: Buckling and postbuckling; elasto-plastic plates; third-order plate theory.

1. Introduction

Many structural elements in various branches of technology can be modeled using a plate model. Buckling is one of the possible collapse modes of slender structural elements and therefore much attention is paid in the literature to the buckling of plates. Important thing to know in order to avoid the structural failure is of course the buckling stress. However, in some cases, it is also useful to follow the postbuckling structural response. Typically, we deal with elastic buckling although for large

§Corresponding author.

loading and specific proportions of stockier structural elements buckling may occur in plastic range. Behavior of low-carbon steels can be modeled with a bilinear constitutive law and explicit yield stress. However, the stainless steels and aluminum alloys exhibit nonlinear behavior with the plastic strains appearing even for relatively small stresses.

Many papers focused on comparison of incremental and deformation theories. Shrivastava[1] analyzed the inelastic buckling by including the effects of transverse shear by deformation and incremental theories of plasticity. Owen and Figueiras[2] used a thick shell formulation accounting for shear deformation based on a degenerate three-dimensional continuum element. Watanabe and Kondo[3] formulated the elastic-plastic incremental tangent stiffness matrix without numerical integration over the area of the element deriving increments of the nodal displacements from the yield condition. Ore and Durban[4] presented a linear buckling analysis of annular elasto-plastic plates under shear loads using both plasticity theories. Papadopoulos and Taylor[5] derived the discrete field equations from a nonlinear version of the Hu-Washizu variational principle and applied them for a finite element analysis of elasto-plastic Reissner–Mindlin plates. Tugcu[6] analyzed the buckling of elastic-plastic plates subject to biaxial loading using a bifurcation-of-equilibrium approach. Durban and Zuckerman[7] carried out the analysis of rectangular plates under uniaxial loading. The problem of influence of the plate slenderness on the buckling type (elastic versus elastic-plastic) was addressed by Betten and Shin.[8] Wang *et al.*[9] derived analytical elastic/plastic stability criteria for the case of the elastic–plastic buckling of thin and thick plates employing the constitutive equations given by Chakrabarty.[10] Wang and Aung[11] investigated the buckling of thick plates using the Ritz method. The Ritz method was also applied by Smith *et al.*[12] who investigated the plastic buckling of steel plates applying the classical plate theory (CPT). The paper by El-Sawy *et al.*[13] is an example of application of the finite element method to the analysis of the elastic-plastic buckling. Wang and Huang[14] and Zhang and Wang[15] employed the differential quadrature method. This approach was used also by Hasrati *et al.*[16] for postbuckling analysis of compressed plates. Kadkhodayan and Maarefdoust analyzed the elastic/plastic buckling of thin rectangular[17] and skew[18] plates under various loads and boundary conditions using Generalized Differential Quadrature discretization technique. Ruocco[19] solved the differential equations defining the buckling problem of stiffened plates analytically using the Kantorovich technique.

Various deformation theories have been developed for plates. However, in reference to the elastic-plastic analysis, mostly the CPT and the first-order shear deformation theory (FSDT) were used, in the framework of either analytical or numerical approach.

The drawbacks of the CPT and FSDT are well known and have been thoroughly discussed in the literature. These problems can be overcome applying higher-order shear deformation plate theories (HOPT) which offer accurate solution and allow to avoid problems related to first-order theories. The HOPT use higher-order polynomials in the expansion of the displacement components through the thickness of the plate. According to the assumptions of HOPT, the restriction on warping of the

cross section is relaxed and allows for variation in the thickness direction of the plate. Unlike the FSDT, the HOPT require no shear correction factors.

The formulations in the framework of the HOPT can be categorized with respect to various aspects such as the form of expansion of displacements, particularly throughout the thickness, precise fulfilling shear stress free conditions at the top and bottom surfaces and accounting for extensibility of the transverse normal to the mid-surface.

Many of the theories neglect transverse normal strains.[20–27] One of the first formulations which included extensibility of the transverse normal to the mid-surface, significant in the analysis of thick plates and laminated plates with laminae having widely different elastic constants, was proposed by Reissner.[28] Lo *et al.*[29] derived a theory of plates accounting for the effects of transverse shear deformation, transverse normal strain, and a nonlinear distribution of the in-plane displacements with respect to the thickness coordinate. Reissner also combined the distribution of shear stresses through thickness and extensibility of the normal to the midsurface.[30] Other examples of theories including the extensibility can also be found in Refs. 31–35.

Reddy developed a third-order theory with the displacement field capable to describe the quadratic variation of transverse shear strains and stresses and vanishing of transverse shear stresses on the top and bottom surfaces of a plate.[20,36] Leung *et al.*[37] proposed a third-order plate theory releasing the shear-free condition on the top and bottom surfaces. The theory was also applied by Saidi *et al.*[38] to axisymmetric bending and buckling of functionally graded solid circular plates. Jemielita[39] reviewed the governing equations of the refined theories of plates including those developed by Reissner,[40] Schmidt,[41] Levinson,[42] Murthy[43] and Kączkowski[44] including also his own approach.[45] Other examples can be found in Refs. 46–49.

Reddy and Kim[50] formulated a general third-order theory for the plate deformations (GTPT) and demonstrated that it contains the existing plate theories: the general third-order theory with tangential traction free surfaces, the Reddy third-order theory, the first-order plate theory and the CPT. Later they applied the GTPT for the finite element analysis of functionally graded plates with a modified couple stress effect and the von Kármán nonlinearity.[51]

The first to apply the HOPT for the elastic-plastic analysis of bending of plates were Kant *et al.*[52] In their study, they used an HOPT model which included distortion of the transverse normal and used it for the elasto-plastic analysis of plate bending, employing the von Mises criterion, associated flow rule and isotropic hardening. The nonlinear equations were solved using the modified Newton–Raphson method. In their development, they also employed the refined higher-order theory formulated by Kant[53] and Kant *et al.*[54] which was also applied by Pandya and Kant to orthotropic plates.[55]

In this paper, some of the displacement-based plate theories are applied to investigate the elastic-plastic analysis of plates in the framework of the finite element method including the buckling and postbuckling effects with the focus on the GTPT. The results are compared to those available in the literature and the authors' own three-dimensional elastic and elastic-plastic analyses using solid finite elements.

2. Deformation Theories Used in the Analysis

2.1. *First-order shear deformation theory*

We begin the presentation with the FSDT based on the displacement field

$$\begin{aligned} u(x,y,z) &= u_m(x,y) + z\theta_x(x,y), \\ v(x,y,z) &= v_m(x,y) + z\theta_y(x,y), \\ w(x,y,z) &= w_m(x,y), \end{aligned} \tag{1}$$

where x and y are coordinates related to the plane where the midsurface is positioned, z is the coordinate perpendicular to x and y, u_m, v_m are in-plane displacements, w_m is an out-of-plane displacement, θ_x and θ_y are rotations of a transverse line and u, v and w are displacement of an arbitrary point. Equation (1) shows that the following Kirchhoff assumptions are valid: the in-plane displacements vary linearly through the plate thickness and the transverse displacement (in the direction perpendicular to the mid-surface) is constant through the thickness which is equivalent to inextensibility of the normal to the midsurface and to vanishing of the normal stresses σ_{zz} — thus, the constitutive relationships are based on the plane stress problem. Regarding the transverse shear stresses the consequence of assuming the displacements according to Eq. (1) is that the transverse normal lines do not remain orthogonal to the midsurface after deformation, thus allowing for transverse shear strains and stresses. The stresses are, however, uniform throughout the thickness which is contrary to the distribution of the transverse shear stresses obtained from 3D elasticity theory which is quadratic and the stresses vanish at the upper and lower plate surfaces. The influence of the uniform shear stress is compensated by introducing a shear correction parameter modifying the shear constitutive relationship.

Since the displacements u, v and w are dependent on the variables u_m, v_m, w_m, θ_x and θ_y application of the theory in the framework of the finite element method calls for C^0 continuity.

Using the displacement field given by Eq. (1), the strains including the nonlinear von Kármán strain components can be derived as follows:

$$\begin{aligned} \varepsilon_{xx} &= \frac{\partial u_m}{\partial x} + \frac{1}{2}\left(\frac{\partial w_m}{\partial x}\right)^2, \\ \varepsilon_{yy} &= \frac{\partial v_m}{\partial y} + \frac{1}{2}\left(\frac{\partial w_m}{\partial y}\right)^2, \\ \varepsilon_{xy} &= \frac{1}{2}\left[\frac{\partial u_m}{\partial y} + \frac{\partial v_m}{\partial x} + z\left(\frac{\partial \theta_x}{\partial y} + \frac{\partial \theta_y}{\partial x}\right) + \frac{\partial w_m}{\partial x}\frac{\partial w_m}{\partial y}\right], \\ \varepsilon_{xz} &= \frac{1}{2}\left[\theta_x + \frac{\partial w_m}{\partial x}\right], \\ \varepsilon_{yz} &= \frac{1}{2}\left[\theta_y + \frac{\partial w_m}{\partial y}\right]. \end{aligned} \tag{2}$$

2.2. *General third-order plate theory*

The third-order plate deformation theories with vanishing surface tractions such as the general third-order theory with tangential traction free surfaces or the Reddy third-order theory have certain drawbacks related to the fact that their formulations require the C^0-interpolation for $u_m, v_m, \theta_x, \theta_y$ and the Hermite interpolation for w_m, θ_z, φ_z. Moreover, in some cases, these theories result in unsymmetrical finite element stiffness matrices even for a linear case.[50] The problem related to various interpolations was addressed by Pandya and Kant[56] who proposed a method of developing an isoparametric displacement finite element formulation including the conditions for vanishing of the transverse shear partly during defining the displacement field as well as when formulating the shear rigidity matrix and used it for the laminated composite plates.

We also note that the condition of vanishing shear stresses at the top and bottom surfaces expressed in an easy manner via shear strains in the elastic range, in the elasto-plasticity range could become more complex due to greater number of nonzero terms in the constitutive matrix.

Reddy and Kim[50] proposed the formulation free from the described limitations. The displacement field for the GTPT is as follows:

$$\begin{aligned} u(x,y,z) &= u_m(x,y) + z\theta_x(x,y) + z^2\varphi_x(x,y) + z^3\psi_x(x,y), \\ v(x,y,z) &= v_m(x,y) + z\theta_y(x,y) + z^2\varphi_y(x,y) + z^3\psi_y(x,y), \\ w(x,y,z) &= w_m(x,y) + z\theta_z(x,y) + z^2\varphi_z(x,y). \end{aligned} \tag{3}$$

Assuming the in-plane displacements u, v in the form of the cubic polynomial and the out-of-plane displacement w in the quadratic polynomial with respect to z we obtain a quadratic variation of the transverse shear in this direction with all the displacements contributing to this distribution. The formulation was employed to derive the equations of motion with the use of the modified couple stress theory for functionally graded material (FGM) plates. The same formulation was also presented[51] for the analysis of the bending deflections of FGM plates. In both cases, the von Kármán nonlinear strains were considered. Similar approach was proposed also by the other authors.[57–59]

In Eq. (3), we have eleven generalized displacements: displacements at the mid-surface u_m, v_m, w_m, rotations of the transverse normal θ_x, θ_y as well as higher order displacements which have more complex physical interpretation $\theta_z, \varphi_x, \varphi_y, \varphi_z, \psi_x, \psi_y$. For instance, θ_z is a constant term in the expression for strain ε_z (and the total strain at the mid-surface):

$$\varepsilon_z = \left.\frac{\partial w}{\partial z}\right|_{z=0} = \theta_z, \tag{4}$$

where φ_z is a multiplier of the linear term of the strain variation

$$\frac{\partial \varepsilon_z}{\partial z} = \frac{\partial^2 w}{\partial z^2} = 2z\varphi_z. \tag{5}$$

The assumed displacement field given by Eq. (3) allows for the parabolic variation of transverse shear strains. The cubic variation of in-plane displacements causes the transverse normal to deteriorate from the straight form while the quadratic variation of out-of-plane displacement implies extension through the thickness thus leading to varying thickness of the plate and emerging direct stresses in the direction of z-coordinate. The von Kármán nonlinear strain–displacement relations obtained by assuming small strains and moderately large rotations can be approximated as follows:

$$\left(\frac{\partial w}{\partial x}\right)^2 \approx \left(\frac{\partial w_m}{\partial x}\right)^2; \quad \left(\frac{\partial w}{\partial y}\right)^2 \approx \left(\frac{\partial w_m}{\partial y}\right)^2; \quad \frac{\partial w}{\partial x}\frac{\partial w}{\partial y} \approx \frac{\partial w_m}{\partial x}\frac{\partial w_m}{\partial y}, \tag{6}$$

with all the remaining quadratic terms equal to 0, leading to the formulation as follows:

$$\begin{aligned}
\varepsilon_{xx} &= \frac{\partial u_m}{\partial x} + z\frac{\partial \theta_x}{\partial x} + z^2\frac{\partial \varphi_x}{\partial x} + z^3\frac{\partial \psi_x}{\partial x} + \frac{1}{2}\left(\frac{\partial w_m}{\partial x}\right)^2,\\
\varepsilon_{yy} &= \frac{\partial v_m}{\partial y} + z\frac{\partial \theta_y}{\partial y} + z^2\frac{\partial \varphi_y}{\partial y} + z^3\frac{\partial \psi_y}{\partial y} + \frac{1}{2}\left(\frac{\partial w_m}{\partial y}\right)^2,\\
\varepsilon_{zz} &= \theta_z + 2z\varphi_z,\\
\varepsilon_{xy} &= \frac{1}{2}\left[\frac{\partial u_m}{\partial y} + \frac{\partial v_m}{\partial x} + z\left(\frac{\partial \theta_x}{\partial y} + \frac{\partial \theta_y}{\partial x}\right) + z^2\left(\frac{\partial \varphi_x}{\partial y} + \frac{\partial \varphi_y}{\partial x}\right)\right.\\
&\quad \left. + z^3\left(\frac{\partial \psi_x}{\partial y} + \frac{\partial \psi_y}{\partial x}\right) + \frac{\partial w_m}{\partial x}\frac{\partial w_m}{\partial y}\right],\\
\varepsilon_{xz} &= \frac{1}{2}\left[\theta_x + \frac{\partial w_m}{\partial x} + z\left(2\varphi_x + \frac{\partial \theta_z}{\partial x}\right) + z^2\left(3\psi_x + \frac{\partial \varphi_z}{\partial x}\right)\right],\\
\varepsilon_{yz} &= \frac{1}{2}\left[\theta_y + \frac{\partial w_m}{\partial y} + z\left(2\varphi_y + \frac{\partial \theta_z}{\partial y}\right) + z^2\left(3\psi_y + \frac{\partial \varphi_z}{\partial y}\right)\right].
\end{aligned} \tag{7}$$

We note that applying the shear-free condition becomes straightforward in the case of adopting these assumptions. Developing the formulation toward more complex geometry of the model such as stiffened plates would call for including all nonlinear terms as they can play an important role when the flexural-torsional or tripping buckling modes occur.[60,61]

Considering all relevant aspects we selected the general third-order shear deformation theory described by Eq. (3) to be used to in the elastic-plastic analysis of plates. Kim and Reddy[51] developed a finite element model of the GTPT which requires the use of C^1-continuity. However, the model was used to the modified couple stress theory accounting for the microstructural effect through a single length scale parameter involving the second derivatives of the variables. That problem is not covered in the present analysis and thus adopting

the C^0-approximation for all 11 generalized displacements appears to be an appropriate approach.[50]

2.3. *Three-dimensional analysis*

While isotropic as well as laminated composites and FGM plates are typically analyzed using plate elements, for some cases it can be necessary to apply three-dimensional solid elements with one or several solid elements through the thickness. The use of such elements or 3D analytical solutions may be particularly advantageous when transverse shear effects are predominant and the normal transverse (through thickness) stress should be accounted for. Applying the solid elements, we obtain results which can be used as reference values to verify accuracy of the results obtained with the two-dimensional idealization with using a plate theory. As an example Werner[62] presented a Navier-type three-dimensionally exact solution for bending of linear elastic isotropic rectangular plates. Also Demasi[63] developed a Navier-type method for finding the exact three-dimensional solution for isotropic thick and thin rectangular plates. The formulation was next extended to the case of multilayered plates composed of isotropic layers.[64] Zenkour[65,66] applied the 3D analytical elasticity solutions as a reference for functionally graded plates. A comparison of results according to the Mindlin and Reddy plate models with three-dimensional solutions for elastic simply supported isotropic and transverse inextensible rectangular plate can be found in Ref. 67.

The 3D analysis allows for the application of a fully three-dimensional elastic and elastic-plastic constitutive equations, similarly as in the GTPT. Thus, the transverse direct and shear stresses in this case are calculated directly without assumptions regarding the kinematics of deformations which provides a distribution of stresses close to reality.

In the present analysis, the nonlinear strain–displacement equations involving all nonlinear terms typically used for the geometrically nonlinear analysis with the application of a solid element are replaced by the von Kármán equations to retain consistency with the formulations for the plate model:

$$\begin{aligned}
\varepsilon_{xx} &= \frac{\partial u}{\partial x} + \frac{1}{2}\left(\frac{\partial w}{\partial x}\right)^2, \\
\varepsilon_{yy} &= \frac{\partial v}{\partial y} + \frac{1}{2}\left(\frac{\partial w}{\partial y}\right)^2, \\
\varepsilon_{zz} &= \frac{\partial w}{\partial z}, \\
\gamma_{xy} &= \frac{\partial u}{\partial y} + \frac{\partial v}{\partial x} + \frac{\partial w}{\partial x}\frac{\partial w}{\partial y}, \\
\gamma_{xz} &= \frac{\partial w}{\partial x} + \frac{\partial u}{\partial z}, \\
\gamma_{yz} &= \frac{\partial w}{\partial y} + \frac{\partial v}{\partial z}.
\end{aligned} \tag{8}$$

3. Finite Element Formulation

3.1. *Derivation of equilibrium equation*

Nonlinear finite element equations in the incremental formulation are derived using the principle of virtual work which for increment $t + \Delta t$ and iteration $i + 1$ is given by

$$\delta_{i+1}^{t+\Delta t} W_{\text{int}} = \delta_{i+1}^{t+\Delta t} W_{\text{ext}}, \tag{9}$$

where $\delta_{i+1}^{t+\Delta t} W_{\text{ext}}$ is the virtual work of external forces for an increment $t + \Delta t$ and iteration $i + 1$

$$\delta_{i+1}^{t+\Delta t} W_{\text{ext}} = \int_V {}_{i+1}^{t+\Delta t} b_i \delta_{i+1}^{t+\Delta t} u_i \mathrm{d}V + \int_\Omega {}_{i+1}^{t+\Delta t} p_i \delta_{i+1}^{t+\Delta t} u_i \mathrm{d}\Omega, \tag{10}$$

where $\mathbf{b}$ is the vector of the body forces acting in volume V, p is the loading distributed over area Ω, while u denotes the displacement functions dependent on the formulation corresponding to either the plate theory or the solid formulation.

Virtual work of internal forces (second Piola–Kirchhoff stresses) $\delta_{i+1}^{t+\Delta t} W_{\text{int}}$ has the form as follows:

$$\delta_{i+1}^{t+\Delta t} W_{\text{int}} = \int_V {}_{i+1}^{t+\Delta t} \sigma_{ij} \delta_{i+1}^{t+\Delta t} \Delta\varepsilon_{ij} \mathrm{d}V. \tag{11}$$

Increments of the Green–Lagrange strains ${}_{i+1}^{t+\Delta t}\Delta\varepsilon$ assuming large displacements can be derived using von Kármán nonlinear strain–displacement relations.

Applying the finite element approximation and introducing strain–displacement matrices, $\mathbf{B}^{(1)}$ and $\mathbf{B}^{(2)}$, the increments of the strains, are derived from the strains defined by Eqs. (2), (7), and (8).

$${}_{i+1}^{t+\Delta t}\Delta\varepsilon_{ij} = {}_{i}^{t+\Delta t}\mathbf{B}_{ijk}^{(1)} i+1^{t+\Delta t}\Delta d_k + {}_{i}^{t+\Delta t}\mathbf{B}_{ijkl}^{(2)} i+1^{t+\Delta t}\Delta d_k {}_{i+1}^{t+\Delta t}\Delta d_l, \tag{12}$$

where d are nodal displacements. The strain increments and matrices $\mathbf{B}^{(1)}$ and $\mathbf{B}^{(2)}$ are given in appendix. The stress increments are evaluated using the constitutive relationship as follows:

$${}_{i+1}^{t+\Delta t}\Delta\sigma_{ij} = {}_{i}^{t+\Delta t} D_{ijkl} {}_{i+1}^{t+\Delta t}\Delta\varepsilon_{kl}. \tag{13}$$

The principle of virtual work using Eqs. (11)–(14) takes the form as follows:

$$({}_{i}^{t+\Delta t}K_{pk}^{(d)} + {}_{i}^{t+\Delta t}K_{pk}^{(S)}) {}_{i+1}^{t+\Delta t}\Delta d_k = ({}_{i}^{t+\Delta t}\lambda^{(P)} + {}_{i+1}^{t+\Delta t}\Delta\lambda^{(P)}) P_p - {}_{i}^{t+\Delta t}F_p, \tag{14}$$

where

$${}_{i}^{t+\Delta t}K_{pq}^{(d)} = \int_V {}_{i}^{t+\Delta t} D_{ijkl} {}^{t}{}_{i} B_{ijp}^{(1)} i^{t+\Delta t} B_{klq}^{(1)} \mathrm{d}V, \tag{15}$$

is the stiffness matrix dependent on displacements (including also the linear term)

$${}_{i}^{t+\Delta t}K_{pq}^{(S)} = \int_V ({}_{i}^{t+\Delta t}B_{ijqp}^{(2)} + {}_{i}^{t+\Delta t} B_{ijpq}^{(2)}) {}_{i}^{t+\Delta t}\sigma_{ij} \mathrm{d}V, \tag{16}$$

is the stiffness matrix dependent on stresses,

$$P_p = \int_V b_i N_{ip} \mathrm{d}V + \int_\Omega p_i N_{ip} \mathrm{d}\Omega, \tag{17}$$

is the reference load vector, and

$${}^{t+\Delta t}_{i}F_p = \int_V {}^{t+\Delta t}_{i}B^{(1)}_{ijp}\, i^{t+\Delta t}\sigma_{ij} \mathrm{d}V, \tag{18}$$

is the internal force vector.

The buckling stress (bifurcation point) is found from the condition

$$\det({}^{t+\Delta t}_{i}\mathbf{K}^{(d)} + {}^{t+\Delta t}_{i}\mathbf{K}^{(S)}) = 0. \tag{19}$$

The structural response in the postbuckling regime was analyzed applying the path-following technique in the form of the Crisfield constant arc-length method by adopting a constraint condition in addition to the equation set. The constraint delimiting the displacement increment in each load step ${}^{t+\Delta t}_{i+1}\Delta\mathbf{d}_{\mathrm{incr}}$ is expressed by

$$({}^{t+\Delta t}_{i+1}\Delta\mathbf{d}_{\mathrm{incr}})^T\, {}^{t+\Delta t}_{i+1}\Delta\mathbf{d}_{\mathrm{incr}} = \Delta l^2. \tag{20}$$

3.2. *Finite elements for plate models*

In the present analyses, the FSDT and GTPT were employed. The finite element used for the plate is a sixteen-noded isoparametric Mindlin plate finite element of the Lagrange family with Lobatto numerical integration, which is free from shear locking[68] and thus also adequate for the analysis thin plates. Shape functions for the plate element are as follows:

$$N^{(P)}_{IJ}(\xi,\eta) = N^{(L)}_I(\xi) N^{(L)}_J(\eta), \tag{21}$$

where $N^{(L)}_I(\xi)$ are the shape functions derived using the one-dimensional Lagrange polynomials, and taking the location of the integration points according to the Lobatto quadrature $\xi_1 = -1, \xi_2 = -1/\sqrt{5}, \xi_3 = 1/\sqrt{5}, \xi_4 = 1$:

$$\begin{aligned}
N^{(L)}_1(\xi) &= -\frac{1}{8}(5\xi^3 - 5\xi^2 - \xi + 1),\\
N^{(L)}_2(\xi) &= \frac{5}{8}(\xi^3\sqrt{5} - \xi^2 - \xi\sqrt{5} + 1),\\
N^{(L)}_3(\xi) &= -\frac{5}{8}(\xi^3\sqrt{5} + \xi^2 - \xi\sqrt{5} - 1),\\
N^{(L)}_4(\xi) &= \frac{1}{8}(5\xi^3 + 5\xi^2 - \xi - 1).
\end{aligned} \tag{22}$$

More details are given in Ref. 68 where the results of the patch tests are presented and it is shown that the element is free from shear locking thus being adequate for the analysis of thin plates.

3.3. *Finite elements for solid model*

The 27-noded and 64-noded hexahedral elements are used to set up models for the analysis of bending and buckling of plates. To achieve appropriate accuracy, it is necessary to keep the element aspect ratio as close as possible to a regular cubic form. Moreover, the number of elements in the thickness direction is important for the solution accuracy in thick plates. The 27-noded element was discussed in Ref. 69 while the 64-noded solid element was developed specifically here for the purpose of comparative analysis with the third-order plate theory as an extension of the 16-noded plate element in the third direction. The Lobatto integration technique was also employed for this element as the position of the Lobatto points allows to investigate the value of shear stress on the delimiting surfaces. The shape functions are a natural expansion of the functions defined in Eqs. (21) and (22) are as follows:

$$N_{IJK}^{(S)}(\xi,\eta,\zeta) = N_I^{(L)}(\xi)N_J^{(L)}(\eta)N_K^{(L)}(\zeta). \tag{23}$$

The formulation allows to investigate the stresses at the boundaries (in this case the delimiting top and bottom surfaces) to specifically verify the value of the shear stress there.

4. Material Model

The material behavior is modeled by the Ramberg–Osgood elastoplastic stress–strain relationship assumed in the form

$$\varepsilon_e = \frac{\sigma_e}{E} + k\frac{\sigma_Y}{E}\left(\frac{\sigma_e}{\sigma_Y}\right)^n, \tag{24}$$

where the first term corresponds to the effective elastic strain ε_e^E, while the second to the effective plastic strain ε_e^P, σ_e is the combined stress, σ_Y is the nominal yield stress while k and n are nondimensional parameters defining the shape of the stress–strain elastoplastic curve.

From Eq. (24), we can evaluate the strain hardening parameter as follows:

$$\frac{d\sigma_e}{d\varepsilon_e^P} = \frac{E}{kn}\left(\frac{\sigma_Y}{\sigma_e}\right)^{n-1}. \tag{25}$$

We note that for small values of σ_e the strain hardening has very large value with the infinity for $\sigma_e = 0$. When performing incremental analysis using the finite element method with no-initial-stress condition this singularity can be overcome by assuming the elastic relationship in the initial phase. In fact, in quite large range of stresses the difference of behavior described by the linear equation (the first term of Eq. (22)) and the Ramberg–Osgood model is negligible.

In reference to elastic-plastic response the application of the first-order theory is described in Refs. 9 and 15, following Ref. 10. From equations presented there it follows that the relationships given there are of purely elastic type for the shear stress and strains.

Using an appropriate higher-order deformation theory we can use the kinematic assumption allowing for distribution of shear stresses (true shear stress) and employ constitutive equations resulting from the plastic flow theory. Nevertheless, the results for the first-order shear theory will also be presented.

We note that the constitutive matrix in Eq. (13) is different depending on the plate theory. For the GTPT where there are six stress and strain components it is formed directly from the equations defining the Prandtl–Reuss theory of plasticity while for FSDT the condition of inextensibility in the thickness direction must be used as follows:

$$\Delta\varepsilon_{zz} = 0, \tag{26}$$

which results in a transformation of the constitutive matrix to the form

$$D_{ijkl} = C_{ijkl} - C_{ij33}\frac{C_{33kl}}{C_{3333}}, \tag{27}$$

where

$$C_{ijkl} = 2G\left[1 - \frac{9Gs_{ij}s_{kl}}{2\sigma_y^2(H+3G)}\right].$$

For GTPT, where six stress and strain components are involved, no modification takes place so that

$$D_{ijkl} = C_{ijkl}. \tag{28}$$

5. Numerical Results

5.1. *Verification of the formulation — elastic bending*

The GTPT will be verified comparing the results obtained using this theory with the results obtained using solid elements. Since many results referring to the elastic-plastic behavior plates are obtained using the FSDT, the presented results will also be compared to this theory. Obviously, the principal difference between the FSDT which requires the corrective factor to account for shear stresses and higher order theories which do not require this factor is a possibility to include the shear stresses directly in the constitutive equations upon the condition that the distribution of these stresses correspond to real distribution. Here, it is believed that the "real" distribution of the stresses is provided by the models based on solid elements.

Sixty-four-noded solid elements with the Gauss-Lobatto integration scheme as well as twenty-seven-noded elements are used for the 3D analysis. A simply supported square plate subject to the uniformly distributed loading over the plate area is investigated first. Dimensions of the plate are $b = 800\,\text{mm}$, $t = 80\,\text{mm}$, thus $b/t = 10$ which means a thick plate. The Young modulus of the plate material was assumed equal to $73776.5\,\text{N/mm}^2$ while Poisson ratio 0.32. The loading was $3.90625 \times 10^{-3}\,\text{N/mm}^3$ for the solid model and the equivalent value of $0.3125\,\text{N/mm}^2$

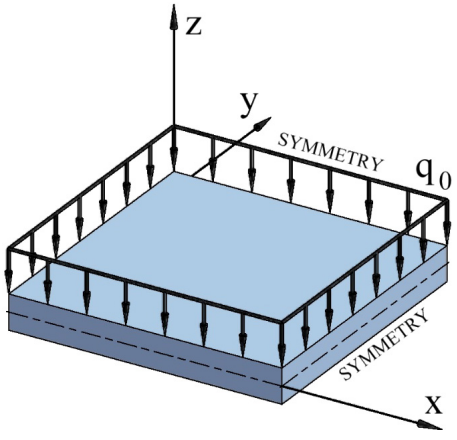

Fig. 1. Simply supported square plate subject to uniform loading.

for the plate model. Both values are the reference values and the actual loading is the reference value multiplied by the loading factor. Meshing was 16×16 for the plate models and $16 \times 16 \times 4$ for the solid models, thus keeping the aspect ratio within reasonable limits. A quarter of the plate was actually modeled (Fig. 1) with the appropriate boundary conditions representing symmetry. We note that for the GTPT these are not only the in-plane displacements and rotations but also the second and third order variables. Regarding the simply supported edges, the kinematic conditions are specified as follows:

$$\begin{aligned} w(0, y) &= 0, \\ w(b, y) &= 0, \\ w(x, 0) &= 0, \\ w(x, b) &= 0, \end{aligned} \tag{29}$$

while the static boundary conditions are as follows:

$$\begin{aligned} m_{xx}(x, 0) &= 0, \\ m_{xx}(x, b) &= 0, \\ m_{yy}(0, y) &= 0, \\ m_{yy}(b, y) &= 0. \end{aligned} \tag{30}$$

Bending moment along edges $y = 0$ and $y = b$ is evaluated as follows:

$$m_{xx} = \int_t \sigma_{xx} z dz, \tag{31}$$

while the normal stress can be found using constitutive relationship

$$\sigma_{xx} = D_{xxxx}\varepsilon_{xx} + D_{xxyy}\varepsilon_{yy} + D_{xxzz}\varepsilon_{zz}. \tag{32}$$

Using the strains components resulting from the displacement field (Eq. (2)), we obtain the following condition:

$$D_{xxxx}\int_t (z^2\theta_{x,x} + z^3\varphi_{x,x} + z^4\psi_{x,x})dz + D_{xxyy}\int_t (z^2\theta_{y,y} + z^3\varphi_{y,y} + z^4\psi_{y,y})dz + D_{xxzz}\int_t (z\theta_z + 2z^2\varphi_z)dz = 0. \tag{33}$$

Thus, to fulfill the condition expressed by Eq. (31) we implement for the edges $y = 0$ and $y = b$:

$$\theta_y = 0, \quad \varphi_y = 0, \quad \psi_y = 0, \quad \theta_z = 0, \quad \varphi_z = 0. \tag{34}$$

Similarly, we apply for the edges $x = 0$ and $x = b$

$$\theta_x = 0, \quad \varphi_x = 0, \quad \psi_x = 0, \quad \theta_z = 0, \quad \varphi_z = 0. \tag{35}$$

Analogous boundary conditions should be applied in the case of the solid element. Since rotations do not appear in the 3D formulation, we insert the boundary conditions $v = 0$ at $x = 0$ and $x = a$ as well as $u = 0$ at $y = 0$ and $y = b$.

As a next step, the loading is changed to cover only a 50×50 mm part of the plate in the center of the plate (patch loading), see Fig. 2. The resultant force is identical as in the previous case which means that the value of loading is now $250 \times 10^{-3}\,\mathrm{N/mm^3}$ for the solid model and the equivalent value of $20\,\mathrm{N/mm^2}$ for the plate model (again both being the reference values). This type of loading induces considerable shear forces and the purpose is to investigate the response of both plate theories to verify the GTPT via comparison with the solid model in the presence of shear forces more significant than in the case of the uniform loading.

Presented results concern nonlinear analysis, both geometrical and material, as the main purpose was the verification of the GTPT for this type of analysis. The results are given for loading factors $\lambda = 1.0$, $\lambda = 40.0$ and $\lambda = 55.0$. The first loading

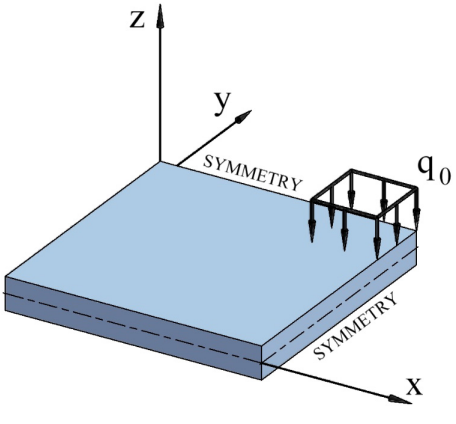

Fig. 2. Simply supported square plate subject to patch loading.

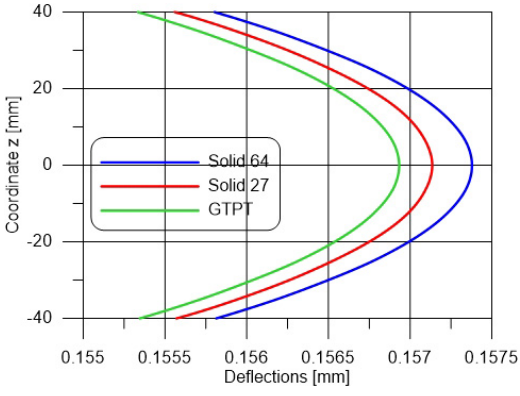

Fig. 3. Distribution of deflections across the thickness for simply supported square plate subject to uniform loading at plate center, $\lambda = 1.0$.

level slightly differs from elastic response with small stresses resulting in positioning the response in the initial part of the Ramberg–Osgood curve and with the deflections not contributing significantly to the geometrically nonlinear response. Two latter loading multipliers are large enough to generate plastic strains as well as more significant geometric effects.

The results in terms of deflections at the center of the plate are given in Fig. 3. We can observe a good agreement of results with the difference between SOLID 64 and GTPT at the level of 0.3%. We can also see a good agreement of results between the two solid models which also confirms correct formulation of the SOLID 64 element proposed in this paper.

In the case of the plate subject to the patch loading, the difference between the deflections is also small, and even if greater than in the previous case it is still less than 1% — Fig. 4.

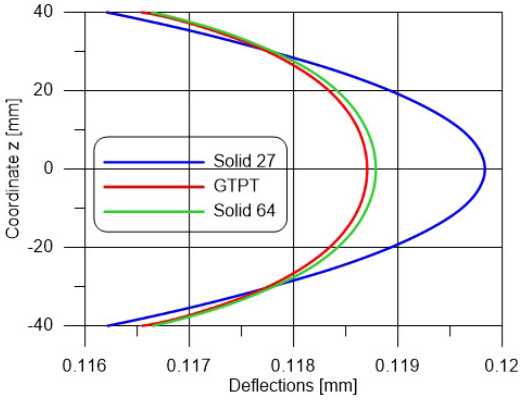

Fig. 4. Distribution of deflections across the thickness for simply supported square plate subject to patch loading at plate center, $\lambda = 1.0$.

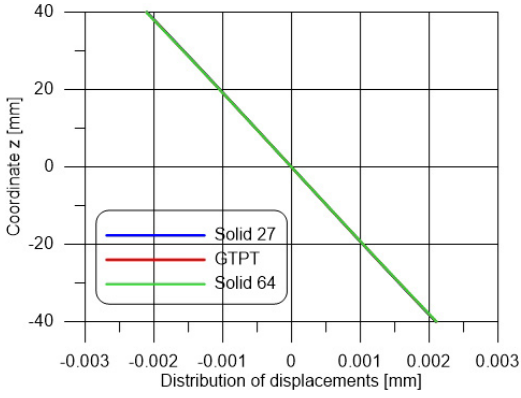

Fig. 5. Distribution of in-plane displacement across the thickness for simply supported square plate subject to uniform loading at $X = Y = 375\,\text{mm}$, $\lambda = 1.0$.

We also note that the deflections obtained using the FSDT are close to the values obtained using the other formulation — 0.1558 mm for the uniform loading and 0.1187 mm for the patch loading.

We also compare distributions of the in-plane displacements across the thickness for coordinates $X = Y = 375\,\text{mm}$ with the displacement in the center obviously equal to 0. We see the excellent agreement of the displacements for both uniform loading (Fig. 5) and patch loading (Fig. 6). In the case of the patch loading, we observe a slightly greater value of the displacement close to the outer surfaces for SOLID 27. However, the agreement of GTPT and SOLID 64 is very good.

Comparing the response of the plates subject to uniform and patch loading we also present the distributions of maximal normal stresses (for outer surface) along the diagonal of the plate. The results are presented in Figs. 7 and 8 in terms of stresses versus the X coordinate.

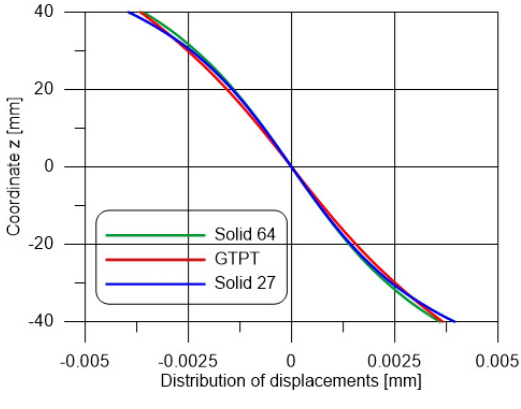

Fig. 6. Distribution of in-plane displacement across the thickness for simply supported square plate subject to patch loading at $X = Y = 375\,\text{mm}$, $\lambda = 1.0$.

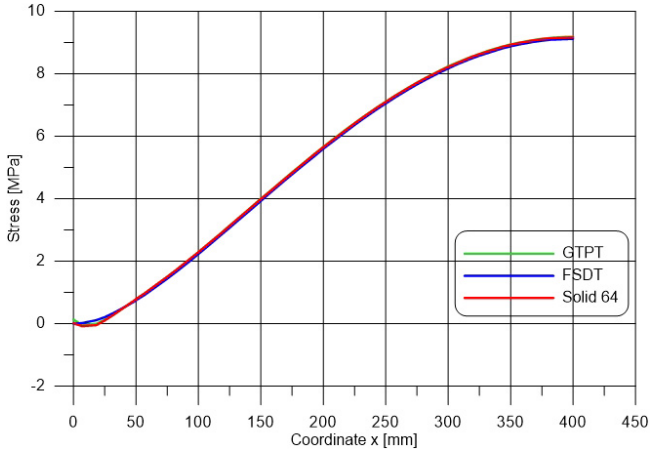

Fig. 7. Distribution of direct stresses for simply supported square plate subject to uniform loading evaluated along diagonal $y = x$ and outer surface $z = 40\,\text{mm}$, $\lambda = 1.0$.

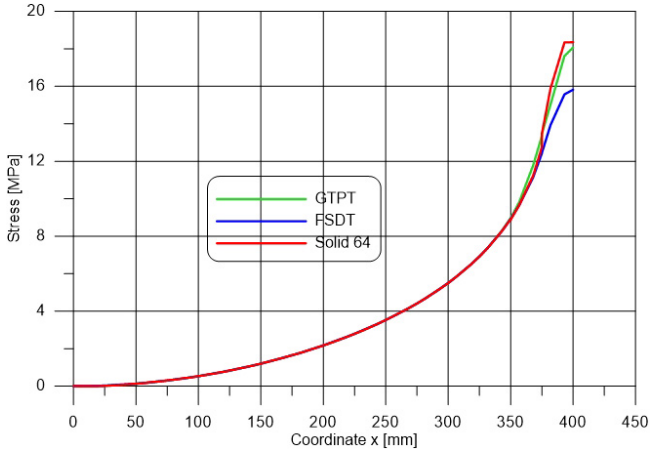

Fig. 8. Distribution of direct stresses for simply supported square plate subject to uniform loading evaluated along the diagonal $y = x$ and outer surface $z = 40\,\text{mm}$, $\lambda = 1.0$.

We observe that the stresses are practically identical in the case of the uniform loading. However, there is a remarkable difference of stresses between the FSDT and GTPT. The GTPT model better follows the stress distribution obtained using the solid model with the difference of maximal stress 1.5% while the FSDT differs by 15%.

We also present the distribution of the maximal midsurface shear stresses along the diagonal, comparing the GTPT to the SOLID 64 model. We can see a good representation of the shear stresses even though in the location of the largest stress — at the border of the patch — the difference is greater, Fig. 9.

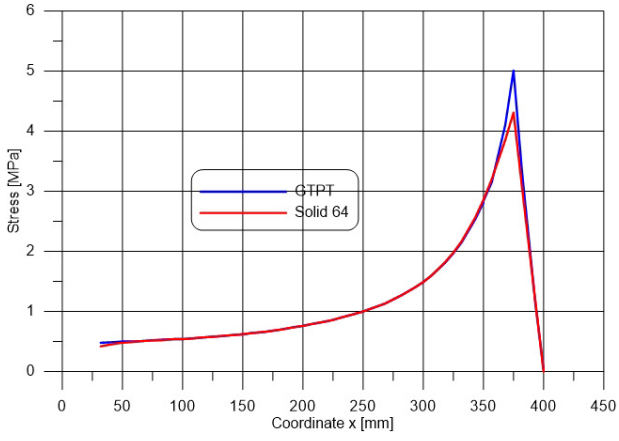

Fig. 9. Distribution of shear stresses for simply supported square plate subject to uniform loading evaluated along the diagonal $y = x$ and midsurface $z = 0\,\text{mm}$, $\lambda = 1.0$.

Distribution of direct stresses for simply supported square plate subject to uniform loading across thickness evaluated at plate center as well as distribution of shear stresses for simply supported square plate subject to uniform loading across thickness at the location of large shear strains ($X = 400\,\text{mm}$, $Y = 50\,\text{mm}$) are presented in Figs. 10 and 11, respectively. We can see the linear distribution of the direct stress corresponding to the elastic response. As it was already mentioned, the load factor $\lambda = 1.0$ despite involving both types of nonlinearity corresponds in fact to the linear response.

An important test of a correct behavior of the plate model is the result of zero shear stresses at the delimiting surfaces. In the GTPT, there is no condition enforcing

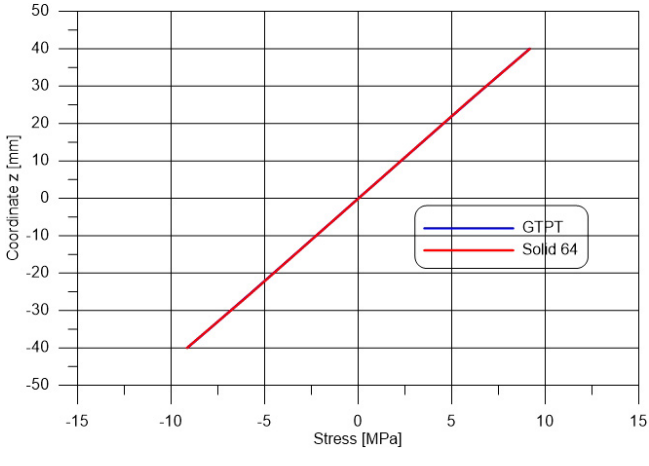

Fig. 10. Distribution of direct stresses for simply supported square plate subject to uniform loading across thickness evaluated at plate center, $\lambda = 1.0$.

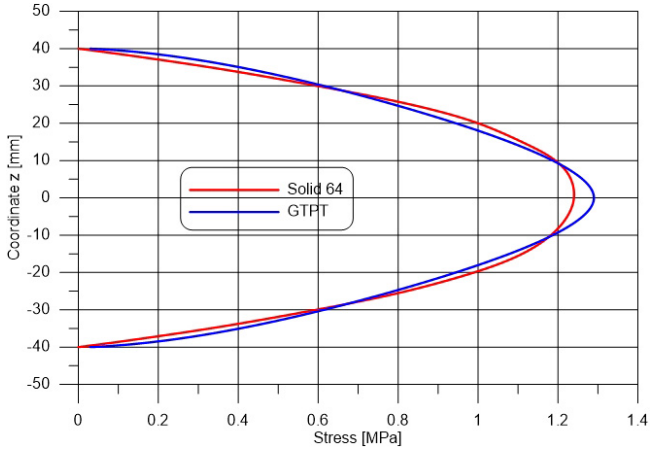

Fig. 11. Distribution of shear stresses for simply supported square plate subject to uniform loading across thickness evaluated at $X = 400\,\text{mm}$, $Y = 50\,\text{mm}$, $\lambda = 1.0$.

these stresses to have zero values and we can see that their values in the required locations are very small (2% of the maximal value) and the distribution follows an expected parabola.

Distributions of stresses for the patch loading are presented in Figs. 12 and 13 for direct and shear stress, respectively. The stresses are present for the same locations as in the case of the uniform loading. Similarly to the results referring to displacements, the distributions differ only slightly. For the normal stress, the agreement is very good, for the shear stress, we observe 10% difference of the maximum values, yet the distribution is parabolic. It should be pointed out, however, that the results are given

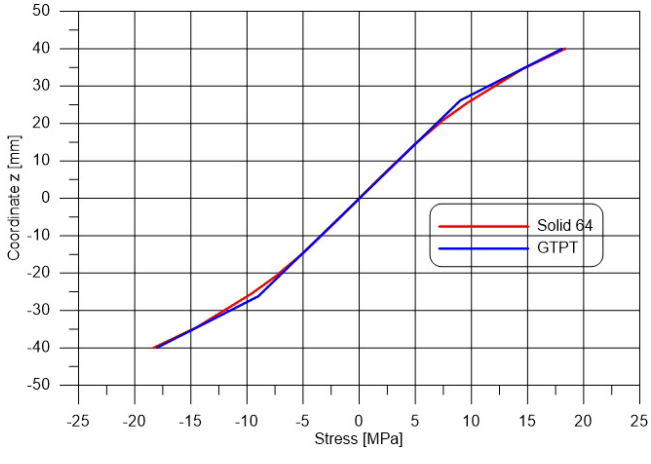

Fig. 12. Distribution of direct stresses for simply supported square plate subject to patch loading across thickness evaluated at plate center, $\lambda = 1.0$.

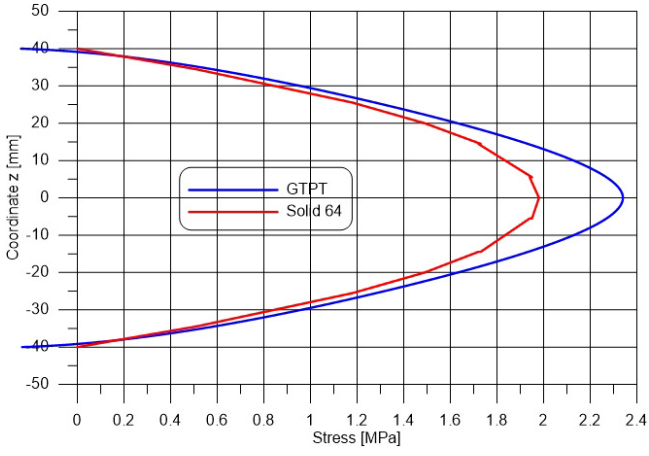

Fig. 13. Distribution of shear stresses for simply supported square plate subject to patch loading across thickness evaluated at $X = 400\,\text{mm}$, $Y = 325\,\text{mm}$, $\lambda = 1.0$.

for the locations with the very large stress gradient and in the remaining part of the plate the difference is definitely less significant.

The conclusion from the elastic analysis is that the GTPT is a good candidate for a theory describing the behavior of thick plates. The elastic-plastic tests follow in the next chapter.

5.2. *Verification of the formulation — elastic-plastic bending*

The geometry of the models and the loading applied for the elastic-plastic analysis are the same as used in the previous chapter. Also the Young modulus ($E = 73,776.5\,\text{N/mm}^2$) and Poisson ratio ($\nu = 0.32$) were identical. Nonlinear material behavior was modeled using the Ramberg–Osgood model with nominal yield stress $\sigma_0 = 423.353\,\text{N/mm}^2$, $n = 20$ and $k = 0.3485$ what corresponds to the 14S-T6 aluminum alloy.

The results are presented for loading factors $\lambda = 55.0$ (uniform loading) and $\lambda = 55.0$ (patch loading). The difference is due to the fact that, even though the resultant forces are identical, the patch loading induces greater stresses. We begin with the presentation of distribution of deflections for the plate center, Figs. 14 and 15.

We see that in the case of elastic-plastic response, the deflections calculated using the GTPT are in a good agreement with the SOLID 64 results. The difference is 0.5% for the uniform loading, again in the case of the patch loading is greater. However, it does not exceed 1.5%.

From results presented in Figs. 16–19 where the distributions of direct and shear stresses are given for uniform and patch loading we can confirm acceptable agreement of results for both types of loading. Regarding the normal stress we observe very good agreement between the SOLID 64 and GTPT models. For the shear stress,

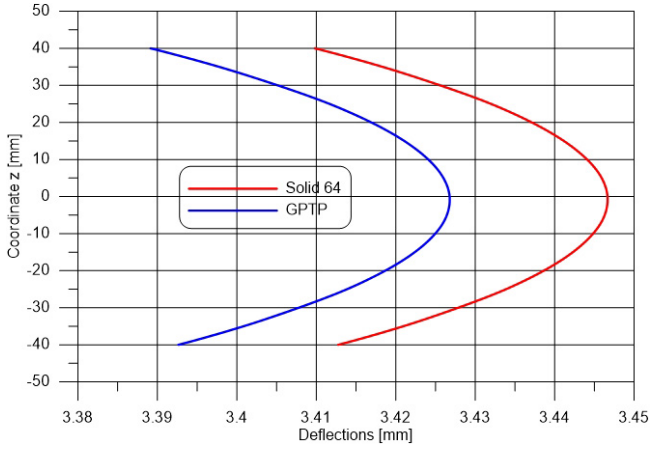

Fig. 14. Distribution of deflections across the thickness for simply supported square plate subject to uniform loading at plate center, $\lambda = 55.0$.

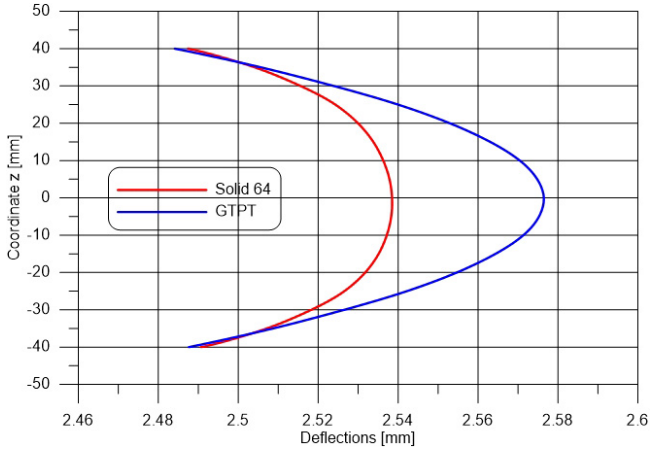

Fig. 15. Distribution of deflections across the thickness for simply supported square plate subject to patch loading at plate center, $\lambda = 55.0$.

we note very good behavior the of SOLID 64 model yielding the values practically zero at these surfaces with the acceptable values for the GTPT.

5.3. *Verification of formulation — buckling*

To verify the correctness of the formulations, we analyze the plate originally investigated by Shrivastava,[1] with the results given also by Wang *et al.*[9] We analyzed square plate subject to uniaxial compressive load. The material of the plate was modeled using the Ramberg–Osgood model with Young modulus equal to $73{,}776.5\,\mathrm{N/mm^2}$ (originally 10,700 ksi), Poisson ratio = 0.32, nominal yield stress

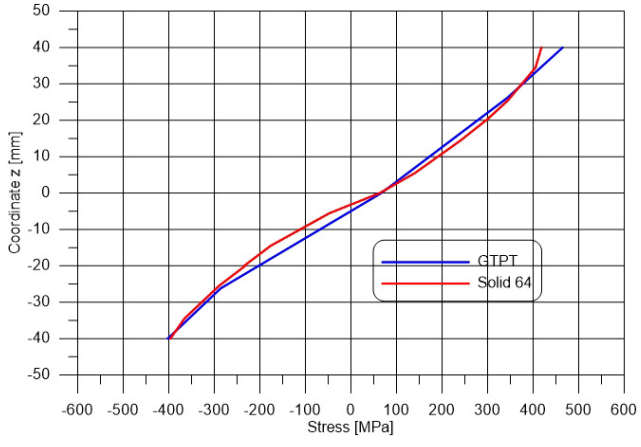

Fig. 16. Distribution of direct stresses for simply supported square plate subject to uniform loading across thickness evaluated at plate center, $\lambda = 55.0$.

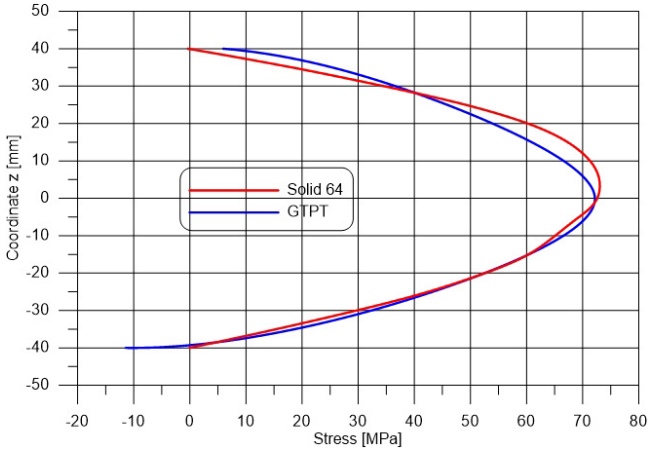

Fig. 17. Distribution of shear stresses for simply supported square plate subject to uniform loading across thickness evaluated at $X = 400\,\text{mm}$, $Y = 50\,\text{mm}$, $\lambda = 55.0$.

$\sigma_0 = 423.353\,\text{N/mm}^2$ (originally $61.4\,\text{ksi}$), $n = 20$ and $k = 0.3485$ corresponding to the 14S-T6 aluminum alloy.

The results of the buckling stress, calculated for the FSDT and GTPT plate theories and the two solid elements: 27-noded and 64-noded, are presented in Table 1 in comparison to those presented by Wang *et al.*[9] according to the incremental theory.

It should be explained that in the case of the solid elements the boundary conditions described in Sec. 5.1. are automatically fulfilled as the displacements at the side surfaces are identical for each y coordinate when the equivalent loading vector is applied evaluated from the pressure acting on the compressed surface of the model.

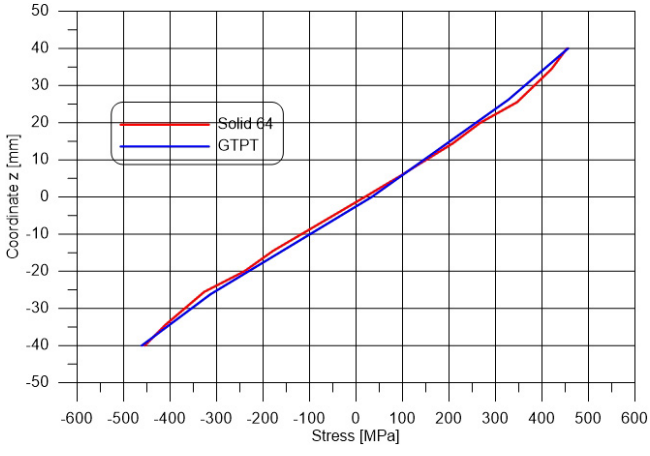

Fig. 18. Distribution of direct stresses for simply supported square plate subject to patch loading across thickness evaluated at plate center, $\lambda = 40.0$.

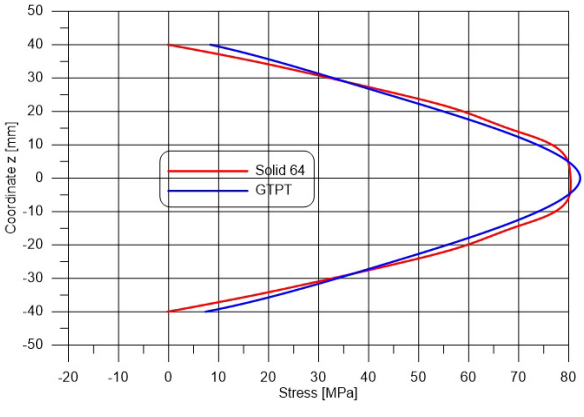

Fig. 19. Distribution of shear stresses for simply supported square plate subject to patch loading across thickness evaluated at $X = 400\,\text{mm}$, $Y = 50\,\text{mm}$, $\lambda = 40.0$.

Table 1. Elastic-plastic buckling stresses for a simply supported, square plate under uniaxial load, MPa.

		Present			
b/t	Wang *et al.*[4]	FSDT	GTPT	Solid 27	Solid 64
22.0	488.45	487.94	488.33	469.53	470.34
23.0	449.30	449.32	449.53	434.69	435.50
24.0	418.60	418.62	418.80	408.09	408.73
25.0	395.50	395.52	395.65	387.53	388.06
26.0	376.44	376.45	376.56	369.40	369.92
27.0	358.10	358.11	358.22	351.00	351.57
28.0	338.62	338.63	338.73	331.21	331.84

We can see a good agreement of results between the GTPT and the reference values of the buckling stress, while for the CPT and FSDT, in the case of thicker plates ($b/t < 25$) the buckling stress is lower and the course of the curve representing relationship buckling stress versus slenderness is different (Fig. 12). We also note slightly less buckling stress in the case of solid model, with the difference ranging from 1.3% to 3.7% comparing to the GTPT but we find the good agreement between the buckling stress for both solid models.

5.4. *Numerical examples*

In order to investigate the influence of boundary conditions, type of loading as well as material characteristics we shall consider several numerical cases involving simply supported and clamped edges with respect to bending as well as restraining effect (blocking midsurface along an edge) and with respect to in-plane displacements, uniaxial and biaxial loading and various stress–strain curves, all in the framework of the Ramberg–Osgood model. We shall also present the nonlinear response of compressed plates in the postbuckling range for various square plate slenderness.

The material of the plate is essentially the same as used in the previous analyses, the Young modulus being equal to $E = 73,776.5\,\mathrm{N/mm^2}$, Poisson ratio $\nu = 0.32$, nominal yield stress $\sigma_0 = 423.353\,\mathrm{N/mm^2}$, $n = 20$ and $k = 0.3485$. Dimensions of the plates are $800 \times 800\,\mathrm{mm}$ with thickness depending on the slenderness.

As the first example we consider again the model presented in Sec. 5.3, the difference being that we take stockier plates exhibiting slenderness of $b/t = 14$ to 20. The comparison of results in terms of the buckling stress is given in Table 2.

The variation of the buckling stress versus slenderness, including also the values from Table 1, is presented in Fig. 20.

We can observe a very good agreement of results for the FSDT and GTPT theories for the plates having slenderness greater than 22 and the difference at the level of up to 5% for the stockier plates. Since the difference between these two theories in the buckling analysis is the inextensibility of the normal transverse in the FSDT and its extensibility in the GTPT we can formulate the conclusion that this is an essential effect for the plates with $b/t < 20$.

In the next study, the influence of the boundary conditions on the buckling stress of the elastic-plastic plate is examined. We continue with the same model as

Table 2. Elastic-plastic buckling stresses for a simply supported, square plate under uniaxial load, MPa.

	Present	
b/t	FSDT	GTPT
14.0	600.15	626.84
16.0	600.14	625.62
18.0	585.77	619.57
20.0	565.08	580.43

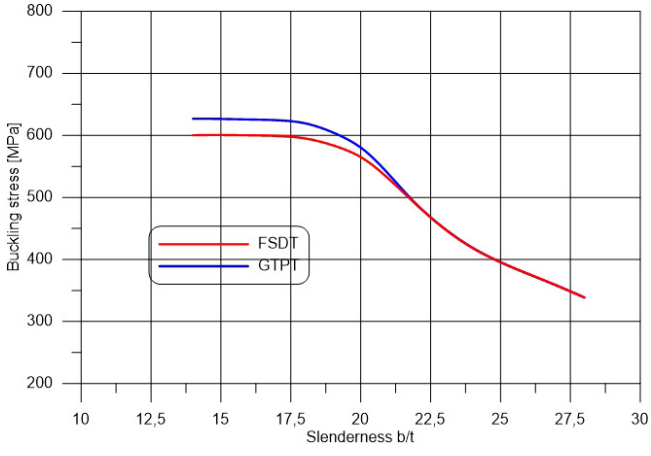

Fig. 20. Buckling stress versus slenderness for simply supported simply supported, square plate under uniaxial load, MPa.

previously and apply various types of boundary conditions on the edges of the plate. First, we compare the behavior of the simply supported plates with the unrestrained and restrained conditions of the midsurface along the edges. In the case of unrestrained boundary conditions, the in-plane displacement u_m of the edges $y = 0$ and $y = b$ as well as the displacement v_m of the edges $x = 0$ and $x = b$ are released while in the case of restrained condition the corresponding displacements are equal to zero. The results in the form of buckling stress versus slenderness for four different cases are presented in Fig. 21.

The unrestrained conditions cause the uniaxially compressive loading which does not generate transversal loading while the restrained conditions generate a biaxial

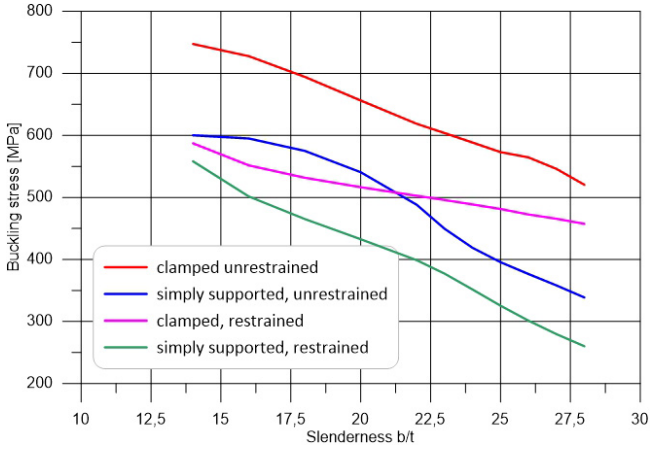

Fig. 21. Buckling stress versus slenderness for simply supported, restrained and unrestrained square plate under uniaxial load, MPa.

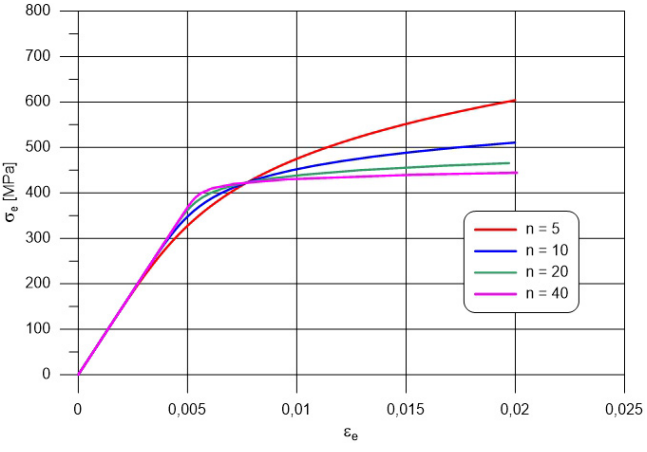

Fig. 22. Stress–strain curves for Ramberg–Osgood material model for various n numbers, MPa.

state of stresses. We note that despite the fact that the response of the plate is stronger, the buckling stresses evaluated using the bifurcation condition are less. The buckling stress decreases with the increase of the slenderness b/t, while for the unrestrained plates the critical stress stabilizes at the value exceeding 600 MPa. We should also note that for the assumed material model the nominal yield stress of 423.3 MPa corresponds to the plastic strain 0.002 while the stress of 470 MPa corresponds to the strain ten times greater so that the buckling stress greater than this value has only a theoretical significance.

We continue presenting our results considering variation of the material parameters. First we investigate the influence of the parameter n on the buckling stress. The Ramberg–Osgood stress–strain curves for values of the parameter ranging from 5 to 40 are shown in Fig. 22.

Figure 23 displays the variation of the buckling stress for the uniaxially compressed plates for four values of the coefficient n (Eq. (24)). They reveal that the buckling stress converges for the plate slenderness greater than 20, where the elastic response dominates effects.

Next the influence of the nominal yield stress, varying from 80% to 120% of the original value. The stress–strain curves for five various nominal yield stresses are shown in Fig. 24. Here, unlike in the previous example, we can see identical shape of the curves in the initial range and a similar one in the part where the equivalent stress is greater than the nominal yield stress.

Variation of the buckling stress depending on the plate slenderness and the nominal yield stress is presented in Fig. 25. The value of the buckling stress decreases with the increase of the plate slenderness. The difference is more apparent for thicker plates where the buckling occurs in the elastic-plastic range while for thinner plates the results converge as the elastic parts of the stress dominate.

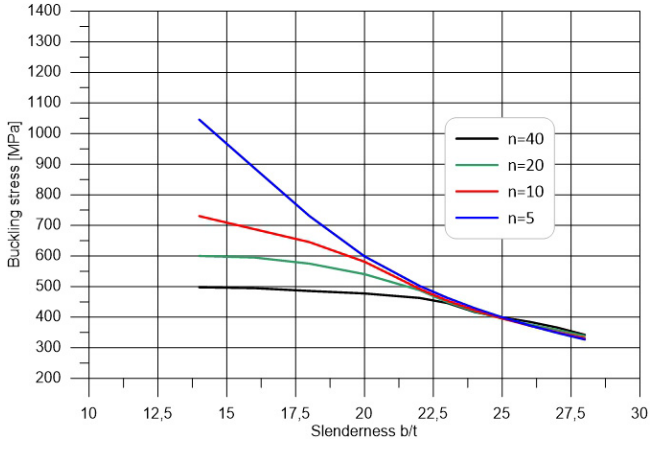

Fig. 23. Buckling stress versus slenderness for simply supported plate under uniaxial load for various n numbers, MPa.

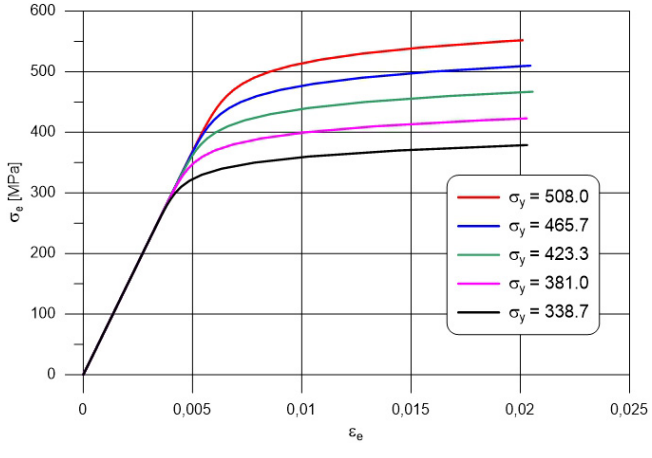

Fig. 24. Stress–strain curves for Ramberg–Osgood material model for various values of yield stress, MPa.

As a next example, we present nonlinear behavior of compressed plates in the postbuckling regime. We investigate the response of three plates having slenderness $b/t = 23$, 26 and 40. The results are presented in Figs. 26–28, respectively in the form of the central deflection versus averaged stress at the compressed edge.

For the plate having slenderness of 23, the buckling stress exceeds the nominal yield stress, so there is practically no reserve of strength and thus we observe the decreasing loading in the postbuckling range.

For the second case of plate with $b/t = 26$ for which the buckling stress is lower than for the unrestrained plate we receive a slight increase of compressive stress. We also note different shapes of the stress–strain curves for the two plates, with unrestrained and restrained in-plane boundary conditions, respectively.

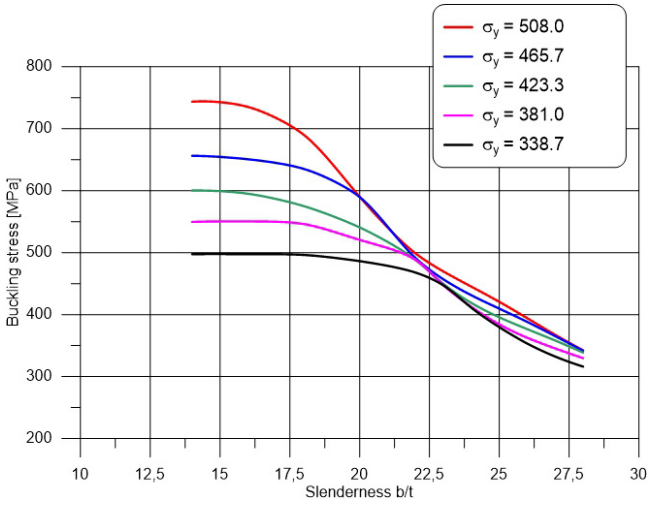

Fig. 25. Buckling stress versus slenderness for simply supported plate under uniaxial load for various values of yield stress, MPa.

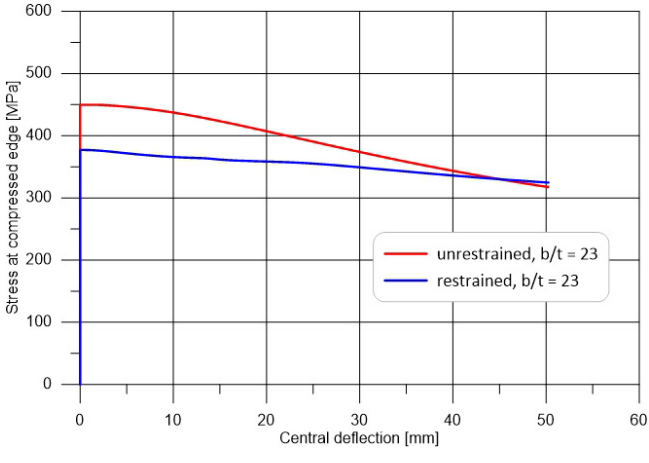

Fig. 26. Stress versus central deflection curve for simply supported, square plate under uniaxial compression, $b/t = 23$.

Interesting behavior can be observed for the plate with slenderness of $b/t = 40$. The buckling stress corresponds to the initial part of the Ramberg–Osgood stress–strain curve which corresponds to buckling.

The nonlinear response for plate with $b/t = 40$ and the restrained in-plane boundary conditions can be explained by observing the deflection modes at particular stages. First the buckling occurs in the mode typical of a square plate, that is one half-sine wave in each direction, see Fig. 29.

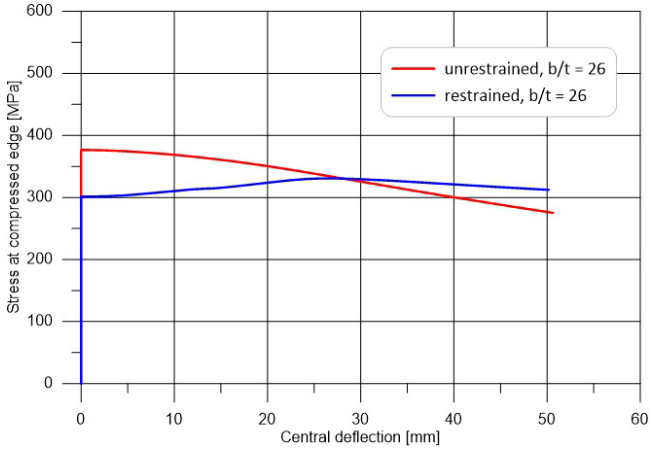

Fig. 27. Stress versus central deflection curve for simply supported, square plate under uniaxial compression, $b/t = 26$.

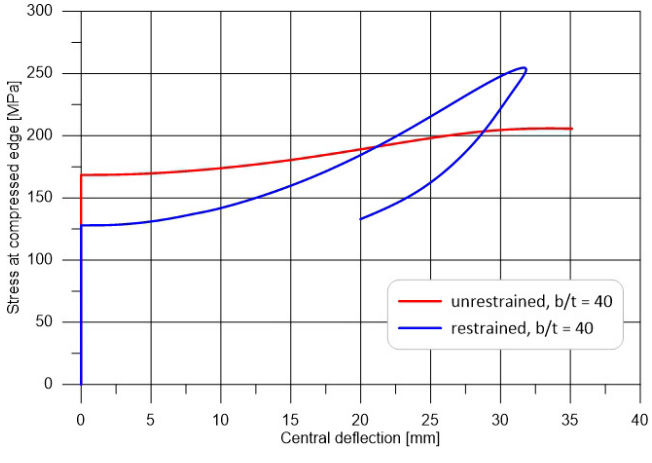

Fig. 28. Stress versus central deflection curve for simply supported, square plate under uniaxial compression, $b/t = 40$.

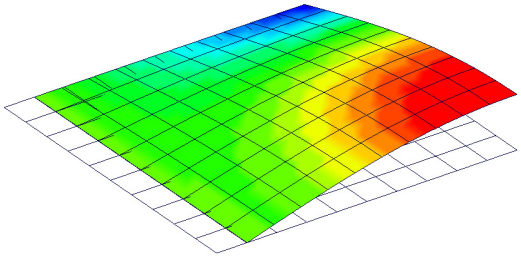

Fig. 29. Elastic buckling mode simply supported and restrained, square plate under uniaxial compression, $b/t = 40$.

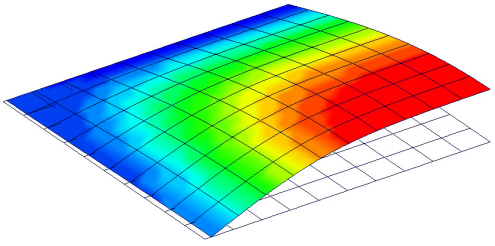

Fig. 30. Deformations for maximum loading for simply supported and restrained, square plate under uniaxial compression, $b/t = 40$.

Increasing the loading in the postbuckling range, we observe transition from the elastic buckling mode to another deformation mode. For the maximum loading, we have deflections as presented in Fig. 30, which should be associated with the ultimate load capacity of the plate.

When we continue the analysis which is possible due to a path-following solution algorithm we observe the change of deformations in the form of a decreasing deflection of the central node, see Fig. 31.

The analysis was terminated when the deflection mode was as presented in Fig. 32.

This example also illustrates the difference between the response of the plates with restrained and unrestrained boundary conditions, as shown in Fig. 21. The unrestrained plate exhibits greater buckling stress, however, this is a restrained plate which reaches greater ultimate capacity in the postbuckling range.

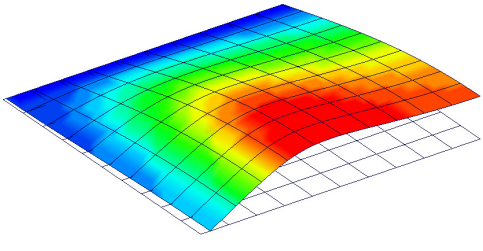

Fig. 31. Deformations for maximum loading for simply supported and restrained, square plate under uniaxial compression, $b/t = 40$.

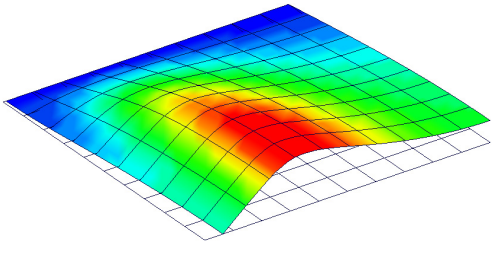

Fig. 32. Deformations for maximum loading for simply supported and restrained, square plate under uniaxial compression, $b/t = 40$.

For the remaining examples referring to stockier plates for which the stress–central deflection curves are presented in Figs. 26 and 27 as well as to the same plate ($b/t = 40$) with unrestrained in-plane boundary conditions, the deflection mode was typical of the buckling mode of a square plate and remained as such throughout the analysis.

6. Concluding Remarks

In this paper, the application of the third order plate deformation theory originally presented by Reddy — the GTPT — was employed for the elastic-plastic analysis of plates using the incremental theory of plasticity with the Prandtl–Reuss constitutive equations and Ramberg–Osgood material model. The approach was verified in a series of numerical tests in which displacements and stress distributions were compared to the results obtained using solid models. The results show good agreement of results and the GTPT can be acknowledged to fulfill essential criteria for the application to the analysis of thick plates. To capture the more practical elastic–plastic behavior, various cases were analyzed with regard to bending of the plates subject to uniform loading and more concentrated loading.

The formulation was also verified by comparing to the results of buckling analysis for the cases where the buckling stresses were given. Again, a good agreement of results has been obtained.

Acknowledgments

The work has been performed under the project functionally graded materials — static and dynamic analyses, financed by the Polish National Science Centre (NCN) under the contract 2018/29/B/ST8/02723. The support is gratefully acknowledged.

Appendix A

The strain increments, evaluated from as the difference between iteration $i+1$ and i, are for the FSDT:

$$
\begin{aligned}
{}^{t+\Delta t}_{i+1}\Delta\varepsilon_x &= {}^{t+\Delta t}_{i+1}\Delta u_{m,x} + z\,{}^{t+\Delta t}_{i+1}\Delta\theta_{x,x} + {}^{t+\Delta t}_{i}w_{m,x}\,{}^{t+\Delta t}_{i+1}\Delta w_{m,x} + \frac{1}{2}({}^{t+\Delta t}_{i+1}\Delta w_{m,x})^2,\\
{}^{t+\Delta t}_{i+1}\Delta\varepsilon_y &= {}^{t+\Delta t}_{i+1}\Delta v_{m,y} + z\,{}^{t+\Delta t}_{i+1}\Delta\theta_{y,y} + {}^{t+\Delta t}_{i}w_{m,y}\,{}^{t+\Delta t}_{i+1}\Delta w_{m,y} + \frac{1}{2}({}^{t+\Delta t}_{i+1}\Delta w_{m,y})^2,\\
{}^{t+\Delta t}_{i+1}\Delta\varepsilon_{xy} &= \frac{1}{2}({}^{t+\Delta t}_{i+1}\Delta u_{m,y} + z\,{}^{t+\Delta t}_{i+1}\Delta\theta_{x,y} + {}^{t+\Delta t}_{i+1}\Delta v_{m,x} + z\,{}^{t+\Delta t}_{i+1}\Delta\theta_{y,x}\\
&\quad + {}^{t+\Delta t}_{i}w_{m,x}\,{}^{t+\Delta t}_{i+1}\Delta w_{m,y} + {}^{t+\Delta t}_{i}w_{m,y}\,{}^{t+\Delta t}_{i+1}\Delta w_{m,x} + {}^{t+\Delta t}_{i+1}\Delta w_{m,x}\,{}^{t+\Delta t}_{i+1}\Delta w_{m,y}),\\
{}^{t+\Delta t}_{i+1}\Delta\varepsilon_{xz} &= \frac{1}{2}({}^{t+\Delta t}_{i+1}\Delta w_{m,x} + {}^{t+\Delta t}_{i+1}\Delta\theta_x),\\
{}^{t+\Delta t}_{i+1}\Delta\varepsilon_{yz} &= \frac{1}{2}({}^{t+\Delta t}_{i+1}\Delta w_{m,y} + {}^{t+\Delta t}_{i+1}\Delta\theta_y).
\end{aligned}
\tag{A.1}
$$

For the GTPT, the strain increments are as follows:

$$
\begin{aligned}
{}^{t+\Delta t}_{i+1}\Delta\varepsilon_{xx} &= {}^{t+\Delta t}_{i+1}\Delta u_{m,x} + z\,{}^{t+\Delta t}_{i+1}\Delta\theta_{x,x} + z^2\,{}^{t+\Delta t}_{i+1}\Delta\varphi_{x,x} + z^3\,{}^{t+\Delta t}_{i+1}\Delta\psi_{x,x} \\
&\quad + {}^{t+\Delta t}_{i}w_{m,x}\,{}^{t+\Delta t}_{i+1}\Delta w_{m,x} + \frac{1}{2}({}^{t+\Delta t}_{i+1}\Delta w_{m,x})^2, \\
{}^{t+\Delta t}_{i+1}\Delta\varepsilon_{yy} &= {}^{t+\Delta t}_{i+1}\Delta v_{m,y} + z\,{}^{t+\Delta t}_{i+1}\Delta\theta_{y,y} + z^2\,{}^{t+\Delta t}_{i+1}\Delta\varphi_{y,y} + z^3\,{}^{t+\Delta t}_{i+1}\Delta\psi_{y,y} \\
&\quad + {}^{t+\Delta t}_{i}w_{m,y}\,{}^{t+\Delta t}_{i+1}\Delta w_{m,y} + \frac{1}{2}({}^{t+\Delta t}_{i+1}\Delta w_{m,y})^2, \\
{}^{t+\Delta t}_{i+1}\Delta\varepsilon_{zz} &= {}^{t+\Delta t}_{i+1}\Delta\theta_z + 2z\,{}^{t+\Delta t}_{i+1}\Delta\varphi_z, \\
{}^{t+\Delta t}_{i+1}\Delta\varepsilon_{xy} &= \frac{1}{2}[{}^{t+\Delta t}_{i+1}\Delta u_{m,y} + {}^{t+\Delta t}_{i+1}\Delta v_{m,x} + z({}^{t+\Delta t}_{i+1}\Delta\theta_{x,y} + {}^{t+\Delta t}_{i+1}\Delta\theta_{y,x}) \\
&\quad + z^2({}^{t+\Delta t}_{i+1}\Delta\varphi_{x,y} + {}^{t+\Delta t}_{i+1}\Delta\varphi_{y,x}) + z^3({}^{t+\Delta t}_{i+1}\Delta\psi_{x,y} + {}^{t+\Delta t}_{i+1}\Delta\psi_{y,x}) \\
&\quad + {}^{t+\Delta t}_{i}w_{m,x}\,{}^{t+\Delta t}_{i+1}\Delta w_{m,y} + {}^{t+\Delta t}_{i}w_{m,y}\,{}^{t+\Delta t}_{i+1}\Delta w_{m,x} + {}^{t+\Delta t}_{i+1}\Delta w_{m,x}\,{}^{t+\Delta t}_{i+1}\Delta w_{m,y}], \\
{}^{t+\Delta t}_{i+1}\Delta\varepsilon_{xz} &= \frac{1}{2}[{}^{t+\Delta t}_{i+1}\Delta\theta_x + {}^{t+\Delta t}_{i+1}\Delta w_{m,x} + z(2\,{}^{t+\Delta t}_{i+1}\Delta\varphi_x + {}^{t+\Delta t}_{i+1}\Delta\theta_{z,x}) \\
&\quad + z^2(3\,{}^{t+\Delta t}_{i+1}\Delta\psi_x + {}^{t+\Delta t}_{i+1}\Delta\varphi_{z,x})], \\
{}^{t+\Delta t}_{i+1}\Delta\varepsilon_{yz} &= \frac{1}{2}[{}^{t+\Delta t}_{i+1}\Delta\theta_y + {}^{t+\Delta t}_{i+1}\Delta w_{m,y} + z(2\,{}^{t+\Delta t}_{i+1}\Delta\varphi_y + {}^{t+\Delta t}_{i+1}\Delta\theta_{z,y}) \\
&\quad + z^2(3\,{}^{t+\Delta t}_{i+1}\Delta\psi_y + {}^{t+\Delta t}_{i+1}\Delta\varphi_{z,y})].
\end{aligned}
\tag{A.2}
$$

For the 3D analysis, the strain increments are follows:

$$
\begin{aligned}
{}^{t+\Delta t}_{i+1}\Delta\varepsilon_{xx} &= {}^{t+\Delta t}_{i+1}\Delta u_{,x} + {}^{t+\Delta t}_{i}w_{,x}\,{}^{t+\Delta t}_{i+1}\Delta w_{,x} + \frac{1}{2}({}^{t+\Delta t}_{i+1}\Delta w_{,x})^2, \\
{}^{t+\Delta t}_{i+1}\Delta\varepsilon_{yy} &= {}^{t+\Delta t}_{i+1}\Delta v_{,y} + {}^{t+\Delta t}_{i}w_{,y}\,{}^{t+\Delta t}_{i+1}\Delta w_{,y} + \frac{1}{2}({}^{t+\Delta t}_{i+1}\Delta w_{,y})^2, \\
{}^{t+\Delta t}_{i+1}\Delta\varepsilon_{zz} &= {}^{t+\Delta t}_{i+1}\Delta w_{,z}, \\
{}^{t+\Delta t}_{i+1}\Delta\varepsilon_{xy} &= \frac{1}{2}({}^{t+\Delta t}_{i+1}\Delta u_{,y} + {}^{t+\Delta t}_{i+1}\Delta v_{,x} + {}^{t+\Delta t}_{i}w_{,x}\,{}^{t+\Delta t}_{i+1}\Delta w_{,y} \\
&\quad + {}^{t+\Delta t}_{i}w_{,y}\,{}^{t+\Delta t}_{i+1}\Delta w_{,x} + {}^{t+\Delta t}_{i+1}\Delta w_{,x}\,{}^{t+\Delta t}_{i+1}\Delta w_{,y}), \\
{}^{t+\Delta t}_{i+1}\Delta\varepsilon_{xz} &= \frac{1}{2}({}^{t+\Delta t}_{i+1}\Delta w_{,x} + {}^{t+\Delta t}_{i+1}\Delta u_{,z}), \\
{}^{t+\Delta t}_{i+1}\Delta\varepsilon_{yz} &= \frac{1}{2}({}^{t+\Delta t}_{i+1}\Delta w_{,y} + {}^{t+\Delta t}_{i+1}\Delta v_{,z}).
\end{aligned}
\tag{A.3}
$$

We apply the finite element approximation of the displacement functions for the FSDT:

$$
\begin{aligned}
u &= N^{(P)}_{1j}d_j, \\
v &= N^{(P)}_{2j}d_j,
\end{aligned}
$$

$$\begin{aligned} w &= N_{3j}^{(P)} d_j, \\ \theta_x &= N_{4j}^{(P)} d_j, \\ \theta_y &= N_{5j}^{(P)} d_j. \end{aligned} \tag{A.4}$$

For the GTPT, we also approximate the remaining displacement functions:

$$\begin{aligned} \theta_z &= N_{6j}^{(P)} d_j, \\ \varphi_x &= N_{7j}^{(P)} d_j, \\ \varphi_y &= N_{8j}^{(P)} d_j, \\ \varphi_z &= N_{9j}^{(P)} d_j, \\ \psi_x &= N_{10j}^{(P)} d_j, \\ \psi_y &= N_{11j}^{(P)} d_j, \end{aligned} \tag{A.5}$$

where $N_{ij}^{(P)}$ are matrices containing shape functions of the 16-noded finite element. With the use of the finite element approximation the strain increments are given in the following generalized form

$$_{i+1}^{t+\Delta t}\Delta\varepsilon_{ij} = {}_{i}^{t+\Delta t}B_{ijk}^{(1)} i + 1^{\,t+\Delta t}\Delta d_k + B_{ijkp}^{(2)} i + 1^{\,t+\Delta t}\Delta d_k \, {}_{i+1}^{t+\Delta t}\Delta d_p, \tag{A.6}$$

where the components of the strain-displacement matrix ${}_{i}^{t+\Delta t}B_{ijp}^{(1)}$ are for the FSDT:

$$\begin{aligned} {}_{i}^{t+\Delta t}B_{11p}^{(1)} &= N_{1p,x}^{(P)} + zN_{4p,x}^{(P)} + N_{3p,x}^{(P)} N_{3k,x}^{(P)} \, i^{t+\Delta t} d_k, \\ {}_{i}^{t+\Delta t}B_{22p}^{(1)} &= N_{2p,y}^{(P)} + zN_{5p,y}^{(P)} + N_{3p,y}^{(P)} N_{3k,y}^{(P)} i^{t+\Delta t} d_k, \\ {}_{i}^{t+\Delta t}B_{12p}^{(1)} &= \frac{1}{2}[N_{1p,y}^{(P)} + N_{2p,x}^{(P)} + z(N_{4p,y}^{(P)} + N_{5p,x}^{(P)}) + (N_{3p,x}^{(P)} N_{3k,y}^{(P)} + N_{3p,y}^{(P)} N_{3k,x}^{(P)}) {}_{i}^{t+\Delta t} d_k], \\ {}_{i}^{t+\Delta t}B_{13p}^{(1)} &= \frac{1}{2}(N_{3p,x}^{(P)} + N_{4p}^{(P)}), \\ {}_{i}^{t+\Delta t}B_{23p}^{(1)} &= \frac{1}{2}(N_{3p,y}^{(P)} + N_{5p}^{(P)}). \end{aligned} \tag{A.7}$$

And for matrix $B_{ijpk}^{(2)}$ the components are as follows:

$$\begin{aligned} B_{11pk}^{(2)} &= \frac{1}{2} N_{3p,x}^{(P)} N_{3k,x}^{(P)}, \\ B_{22pk}^{(2)} &= \frac{1}{2} N_{3p,y}^{(P)} N_{3k,y}^{(P)}, \\ B_{12pk}^{(2)} &= \frac{1}{2} N_{3p,x}^{(P)} N_{3k,y}^{(P)}, \\ B_{13pk}^{(2)} &= 0, \\ B_{23pk}^{(2)} &= 0. \end{aligned} \tag{A.8}$$

For GTPT, the components of the strain-displacement matrix ${}_i^{t+\Delta t}B_{ijp}^{(1)}$ are as follows:

$$\begin{aligned}
{}_i^{t+\Delta t}B_{11p}^{(1)} &= N_{1p,x}^{(P)} + zN_{4p,x}^{(P)} + z^2N_{7p,x}^{(P)} + z^3N_{10p,x}^{(P)} + N_{3p,x}^{(P)}N_{3k,x}^{(P)}\,{}_i^{t+\Delta t}d_k,\\
{}_i^{t+\Delta t}B_{22p}^{(1)} &= N_{2p,y}^{(P)} + zN_{5p,y}^{(P)} + z^2N_{8p,y}^{(P)} + z^3N_{11p,y}^{(P)} + N_{3p,y}^{(P)}N_{3k,y}^{(P)}\,{}_i^{t+\Delta t}d_k,\\
{}_i^{t+\Delta t}B_{33p}^{(1)} &= N_{6p}^{(P)} + 2zN_{9p}^{(P)},\\
{}_i^{t+\Delta t}B_{12p}^{(1)} &= \frac{1}{2}[N_{1p,y}^{(P)} + N_{2p,x}^{(P)} + z(N_{4p,y}^{(P)} + N_{5p,x}^{(P)}) + z^2(N_{7p,y}^{(P)} + N_{8p,x}^{(P)})\\
&\quad + z^3(N_{10p,y}^{(P)} + N_{11p,x}^{(P)}) + (N_{3p,x}^{(P)}N_{3k,y}^{(P)} + N_{3p,y}^{(P)}N_{3k,x}^{(P)})\,{}_i^{t+\Delta t}d_k],\\
{}_i^{t+\Delta t}B_{13p}^{(1)} &= \frac{1}{2}[N_{4p}^{(P)} + N_{3p,x}^{(P)} + z(2N_{7p}^{(P)} + N_{6p,x}^{(P)}) + z^2(3N_{10p}^{(P)} + N_{9p,x}^{(P)})],\\
{}_i^{t+\Delta t}B_{23p}^{(1)} &= \frac{1}{2}[N_{5p}^{(P)} + N_{3p,y}^{(P)} + z(2N_{8p}^{(P)} + N_{6p,y}^{(P)}) + z^2(3N_{11p}^{(P)} + N_{9p,y}^{(P)})].
\end{aligned} \tag{A.9}$$

And the components of ${}_i^{t+\Delta t}B_{ijp}^{(2)}$ are as follows:

$$\begin{aligned}
B_{11pk}^{(2)} &= \frac{1}{2}N_{3p,x}^{(P)}N_{3k,x}^{(P)},\\
B_{22pk}^{(2)} &= \frac{1}{2}N_{3p,y}^{(P)}N_{3k,y}^{(P)},\\
B_{33pk}^{(2)} &= 0,\\
B_{12pk}^{(2)} &= \frac{1}{2}N_{3p,x}^{(P)}N_{3k,y}^{(P)},\\
B_{13pk}^{(2)} &= 0,\\
B_{23pk}^{(2)} &= 0.
\end{aligned} \tag{A.10}$$

Similarly, in the 3D analysis, the components of the strain–displacement matrix ${}_i^{t+\Delta t}B_{ijp}^{(1)}$ are as follows:

$$\begin{aligned}
{}_i^{t+\Delta t}B_{11p}^{(1)} &= N_{1p,x}^{(S)} + N_{3p,x}^{(S)}N_{3k,x}^{(S)}\,{}_i^{t+\Delta t}d_k,\\
{}_i^{t+\Delta t}B_{22p}^{(1)} &= N_{2p,y}^{(S)} + N_{3p,y}^{(S)}N_{3k,y}^{(S)}\,{}_i^{t+\Delta t}d_k,\\
{}_i^{t+\Delta t}B_{33p}^{(1)} &= N_{3p,z}^{(S)},\\
{}_i^{t+\Delta t}B_{12p}^{(1)} &= \frac{1}{2}[N_{1p,y}^{(S)} + N_{2p,x}^{(S)} + (N_{3p,x}^{(S)}N_{3k,y}^{(S)} + N_{3p,y}^{(S)}N_{3k,x}^{(S)})\,{}_i^{t+\Delta t}d_k],\\
{}_i^{t+\Delta t}B_{13p}^{(1)} &= \frac{1}{2}(N_{3p,x}^{(S)} + N_{1p,z}^{(S)}),\\
{}_i^{t+\Delta t}B_{23p}^{(1)} &= \frac{1}{2}(N_{3p,y}^{(S)} + N_{2p,z}^{(S)}).
\end{aligned} \tag{A.11}$$

And the components of ${}^{t+\Delta t}_{i}B^{(2)}_{ijp}$ are as follows:

$$\begin{aligned}
B^{(2)}_{11pk} &= \frac{1}{2}N^{(S)}_{3p,x}N^{(S)}_{3k,x},\\
B^{(2)}_{22pk} &= \frac{1}{2}N^{(S)}_{3p,y}N^{(S)}_{3k,y},\\
B^{(2)}_{33pk} &= 0,\\
B^{(2)}_{12pk} &= \frac{1}{2}N^{(S)}_{3p,x}N^{(S)}_{3k,y},\\
B^{(2)}_{13pk} &= 0,\\
B^{(2)}_{23pk} &= 0.
\end{aligned} \tag{A.12}$$

References

1. S. C. Shrivastava, Inelastic buckling of plates including shear effects, *Int. J. Solids Struct.* **15** (1979) 567–575.
2. D. R. J. Owen and J. A. Figueiras, Anisotropic elasto-plastic finite element analysis of thick and thin plates and shells, *Int. J. Num. Meth. Engng.* **19**(4) (1983) 541–566.
3. N. Watanabe and K. Kondo, A new simplified finite element method for elastic-plastic analysis of plate bending problems, *Comp. Struct.* **28**(4) (1988) 495–503.
4. E. Ore and D. Durban, Elastoplastic buckling of annular plates in pure shear, *J. Appl. Mech.* **56** (1989) 644–651.
5. P. Papadopoulos and R. L. Taylor, Elasto-plastic analysis of Reissner-Mindlin plates, *Appl. Mech. Rev.* **43**(5S) (1990) S40–S50.
6. P. Tugcu, Plate buckling in the plastic range, *Int. J. Mech. Sci.* **33**(1) (1991) 1–11.
7. D. Durban and Z. Zuckerman, Elastoplastic buckling of rectangular plates in biaxial compression/tension, *Int. J. Mech. Sci.* **41** (1999) 751–765.
8. J. Betten and C. H. Shin, Elastic–plastic buckling analysis of rectangular plates subjected to biaxial loads, *Forsch. Ingenieurwes.* **65** (2000) 273–278.
9. C. M. Wang, Y. Xiang and J. Chakrabarty, Elastic/plastic buckling of thick plates, *Int. J. Solids Struct.* **38** (2001) 8617–8640.
10. J. Chakrabarty, *Applied Plasticity* (Springer, New York, 2000).
11. C. M. Wang and T. M. Aung, Plastic buckling analysis of thick plates using p-Ritz method, *Int. J. Solids Struct.* **44** (2007) 6239–6255.
12. S. T. Smith, M. A. Bradford and D. J. Oehlers, Inelastic buckling of rectangular steel plates using a Rayleigh–Ritz method, *Int. J. Struct. Stab. Dyn.* **3**(4) (2003) 503–521.
13. Kh. M. El-Sawy, A. S. Nazmy and M. I. Martini, Elastoplastic buckling of perforated plates under uniaxial compression, *Thin Wall. Struct.* **42** (2004) 1083–1101.
14. X. W. Wang and J. C. Huang, Elastoplastic buckling analyses of rectangular plates under biaxial loadings by the differential quadrature method, *Thin Wall. Struct.* **47** (2009) 14–20.
15. W. Zhang and X. W. Wang, Elastoplastic buckling analysis of thick rectangular plates by using the differential quadrature method, *Comput. Math. Appl.* **61** (2011) 44–61.
16. E. Hasrati, R. Ansari and H. Rouhi, Elastoplastic postbuckling analysis of moderately thick rectangular plates using the variational differential quadrature method, *Aerosp. Sci. Technol.* **91** (2019) 479–493.

17. M. Kadkhodayan and M. Maarefdoust, Elastic/plastic buckling of isotropic thin plates subjected to uniform and linearly varying in-plane loading using incremental and deformation theories, *Aerosp. Sci. Technol.* **32** (2014) 66–83.
18. M. Kadkhodayan and M. Maarefdoust, Elastic/plastic buckling analysis of skew plates under in-plane shear loading with incremental and deformation theories of plasticity by GDQ method, *J. Braz. Soc. Mech. Sci. Eng.* **37** (2015) 761–776.
19. E. Ruocco, Elastoplastic buckling analysis of thin-walled structures, *Aerosp. Sci. Technol.* **43** (2015) 176–190.
20. J. N. Reddy, A simple higher-order theory for laminated composite plates, *J. Appl. Mech.* **51** (1984) 745–752.
21. J. N. Reddy, A refined nonlinear theory of plates with transverse shear deformation, *Int. J. Solids Struct.* **20**(9/10) (1984) 881–896.
22. J. N. Reddy, Analysis of functionally graded plates, *Int. J. Numer. Meth. Engng.* **47** (2000) 663–684.
23. G. Shi, A new simple third-order shear deformation theory of plates, *Int. J. Solids Struct.* **44** (2007) 4399–4417.
24. T. Do, D. Nguyen, N. Duc, H. D. Doan and T. Q. Bui, Analysis of bi-directional functionally graded plates by FEM and a new third-order shear deformation plate theory. *Thin Wall Struct.* **119** (2017) 687–699.
25. N. Wattanasakulpong, G. B. Prusty and D. W. Kelly, Free and forced vibration analysis using improved third-order shear deformation theory for functionally graded plates under high temperature loading, *J. Sandw. Struct. Mater.* **15** (2013) 583–606.
26. I. Shufrin and M. Eisenberger, Stability and vibration of shear deformable plates — first order and higher order analyses, *Int. J. Solids Struct.* **42** (2005) 1225–1251.
27. R. Aghababaei and J. N. Reddy, Nonlocal third-order shear deformation plate theory with application to bending and vibration of plates, *J. Sound Vib.* **326** (2009) 277–289.
28. E. Reissner, On bending of elastic plates, *Q. Appl. Math.* **5**(1) (1947) 55–68.
29. K. H. Lo, R. M. Christensen and E. M. Wu, A high-order theory of plate deformation — Part 1: Homogeneous plates, *J. Appl. Mech.* **44**(4) (1977) 663–668.
30. E. Reissner, A note on bending of plates including the effects of transverse shearing and normal strains, *Z. Angew. Math. Phys.* **32** (1981) 764–767.
31. C. C. Chao, T. P. Chung, C. C. Sheu and J. H. Tseng, A consistent higher-order theory of laminated plates with nonlinear impact modal analysis, *J. Vibrat. Acoust.* **116** (1994) 371–378.
32. K. P. Soldatos and P. Watson, Accurate stress analysis of laminated plates combining two-dimensional theory with the exact three-dimensional solution for simply supported edges, *Math. Mech. Solids* **2** (1997) 459–489.
33. C. S. Babu and T. Kant, Refined higher-order finite element models for thermal buckling of laminated composites and sandwich plates, *J. Therm. Stresses* **23** (2000) 111–130.
34. R. C. Batra and S. Vidoli, Higher-order piezoelectric plate theory derived from a three-dimensional variational principle, *AIAA J.* **40** (2002) 91–104.
35. R. C. Batra and S. Aimmanee, Vibrations of thick isotropic plates with higher order shear and normal deformable plate theories, *Comput. Struct.* **83**(12–13) (2005) 934–955.
36. J. N. Reddy, A general non-linear third-order theory of plates with moderate thickness, *Int. J. Nonlin. Mech.* **25**(6) (1990) 677–686.
37. A. Y. T. Leung, N. Junchuan, C. W. Lim and S. Kongjie, A new unconstrained third-order plate theory for Navier solutions of symmetrically laminated plates, *Comput. Struct.* **81** (2003) 2539–2548.

38. A. R. Saidi, A. Rasouli and S. Sahraee, Axisymmetric bending and buckling analysis of thick functionally graded circular plates using unconstrained third-order shear deformation plate theory, *Compos. Struct.* **89** (2009) 110–119.
39. G. Jemielita, On Kinematical assumptions of refined theories of plates: A survey, *J. Appl. Mech.* **57** (1990) 1088–1091.
40. E. Reissner, On transverse bending of plates, including the effect of transverse shear deformation, *Int. J. Solids Struct.* **11** (1975) 569–573.
41. R. Schmidt, A refined nonlinear theory for plates with transverse shear deformations, *J. Ind. Math. Soc.* **27**(1) (1977) 23–38.
42. M. Levinson, An accurate, simple theory of statics and dynamics of elastic plates, *Mech. Res. Comm.* **7**(6) (1980) 342–350.
43. M. V. V. Murthy, An improved transverse shear deformation theory for laminated anisotropic plates, 1981, NASA Technical Paper 1903.
44. Z. Kączkowski, *Plates: Static Calculations* (Arkady, Warszawa, 1968) (in Polish).
45. G. Jemielita, Technical theory of plates of moderate thickness, *Engng. Trans.* **23**(3) (1975) 483–499 (in Polish).
46. A. V. Krishna Murty, Higher order theory for vibrations of thick plates, *AIAA J.* **15**(12) (1977) 1823–1824.
47. A. V. Krishna Murty, Toward a consistent plate theory, *AIAA J.* **24**(6) (1986) 1047–1048.
48. T. Lewinski, On refined plate models based on kinematical assumptions, *Ingenieur Archiv.* **57**(2) (1987) 133–146.
49. A. V. Krishna Murty and S. Vellaichamy, Higher-order theory of homogeneous plate flexure, *AIAA J.* **26**(6) (1988) 719–725.
50. J. N. Reddy and J. Kim, A nonlinear modified couple stress-based third-order theory of functionally graded plates, *Compos Struct.* **94** (2012) 1128–1143.
51. J. Kim and J. N. Reddy, A general third-order theory of functionally graded plates with modified couple stress effect and the von Kármán nonlinearity: Theory and finite element analysis, *Acta Mech.* **226** (2015) 2973–2998.
52. T. Kant, R. K. Tripathi and V. Rode, Elasto-plastic behaviour of thick plates with a higher-order shear, *Proc. Indian Natn. Sci. Acad.* **79**(4) (2013) 563–574.
53. T. Kant, Numerical analysis of thick plates, *Comput. Method Appl. M.* **31**(1) (1982) 1–18.
54. T. Kant, D. R. J. Owens and O. C. Zienkiewicz, A refined higher-order C° plate bending element, *Comp. Struct.* **15**(2) (1982) 177–183.
55. B. N. Pandya and T. Kant, A refined higher-order generally orthotropic co plate bending element, *Comp. Struct.* **28**(2) (1988) 119–133.
56. B. N. Pandya and T. Kant, A simple finite element formulation of a higher-order theory for unsymmetrically laminated composite plates, *Compos. Struct.* **9**(3) (1988) 215–246.
57. A. M. A. Neves, A. J. M. Ferreira, E. Carrera, M. Cinefra, C. M. C. Roque, R. M. N. Jorge and C. M. M. Soares, Static, free vibration and buckling analysis of isotropic and sandwich functionally graded plates using a quasi-3D higher-order shear deformation theory and a meshless technique, *Compos. Part B-Eng.* **44** (2013) 657–674.
58. E. Carrera, Developments, ideas, and evaluations based upon Reissner's mixed variational theorem in the modelling of multilayered plates and shells, *Appl. Mech. Rev.* **54** (2001) 301–329.
59. E. Carrera, Theories and finite elements for multilayered plates and shells: A unified compact formulation with numerical assessment and benchmarking, *Arch. Comput. Methods Eng.* **10** (2003) 215–296.
60. E. Ruocco, Elastic/plastic buckling of moderately thick plates and members, *Comp. Struct.* **158** (2015) 148–166.

61. M. Taczała, R. Buczkowski and M. Kleiber, Nonlinear buckling and post-buckling response of stiffened FGM plates in thermal environments, *Compos. Part B-Eng.* **109** (2017) 238–247.
62. H. Werner, A three-dimensional solution for rectangular plate bending free of transversal normal stresses, *Commun. Numer. Meth. Engng.* **15** (1999) 295–302.
63. L. Demasi, Three-dimensional closed form solutions and exact thin plate theories for isotropic plates, *Compos. Struct.* **80** (2007) 183–195.
64. L. Demasi, 2D, quasi 3D and 3D exact solutions for bending of thick and thin sandwich plates, *J. Sandw. Struct. Mater.* **10** (2008) 271–310.
65. A. M. Zenkour, Generalized shear deformation theory for bending analysis of functionally graded plates, *Appl. Math. Model.* **30** (2006) 67–84.
66. A. M. Zenkour, Benchmark trigonometric and 3-D elasticity solutions for an exponentially graded thick rectangular plate, *Arch. Appl. Mech.* **77** (2007) 197–214.
67. M. Batista, Comparison of Reissner, Mindlin and Reddy plate models with exact three dimensional solution for simply supported isotropic and transverse inextensible rectangular plate, *Meccanica* **47** (2012) 257–268.
68. R. Buczkowski, M. Taczała and M. Kleiber, A 16-node locking-free Mindlin plate resting on two-parameter elastic foundation — static and eigenvalue analysis, *Comput. Assist. Meth. Eng. Sci.* **22** (2015) 99–114.
69. O. C. Zienkiewicz, R. L. Taylor and J. Z. Zhu, *The Finite Element Method: Its Basis and Fundamentals*, 7th edn. (Butterworth-Heinemann, Elsevier, Amsterdam, 2013).